ADVANCED MATERIALS
www.advmat.de

Advanced Materials for Zinc-Based Flow Battery: Development and Challenge

*Zhizhang Yuan, Yanbin Yin, Congxin Xie, Huamin Zhang, Yan Yao, and Xianfeng Li**

Dedicated to the Dalian Institute of Chemical Physics, Chinese Academy of Sciences on the occasion of its 70th anniversary

Zinc-based flow batteries (ZFBs) are well suitable for stationary energy storage applications because of their high energy density and low-cost advantages. Nevertheless, their wide application is still confronted with challenges, which are mainly from advanced materials. Therefore, research on advanced materials for ZFBs in terms of electrodes, membranes, and electrolytes as well as their chemistries are of the utmost importance. Herein, the focus is on the scientific understandings of the fundamental design of these advanced materials and their chemistries in relation to the battery performance. The principles of using different materials in different ZFB technologies, the functions and structure of the materials, and further material improvements are discussed in detail. Finally, the challenges and prospects of ZFBs are summarized as well. This review provides valuable instruction on how to design and develop new materials as well as new chemistries for ZFBs.

1. Introduction

Renewable energies such as solar and wind power have become increasingly important due to the crises of energy shortage and high environmental load.[1–3] However, these renewables are intermittent in nature, which is one of the obstacles hindering their widespread application. Energy storage devices, particularly electrochemical energy storage technology, participate in extremely extensive applications ranging from improving the stability and efficiency of the electric grid to portable electronic devices as well as supplying backup power in districts with limited grid connectivity or in off-grid applications,[4–7] are an effective approach to address these issues.

Among the numerous electrochemical energy storage techniques, flow batteries (FBs) are well suited for energy storage because of their perfect combination of high safety, high efficiency and flexibility.[8–10] A flow battery realizes the transformation of chemical energy into electric energy through the oxidation and reduction reactions of redox couples stored in electrolytes that typically circulate through the anode and cathode, which are normally separated by an ion-conducting membrane.[11] Compared with other battery systems such as lithium-based batteries and lead-based batteries, the power of a flow battery is determined by the size and number of cell stacks, while the energy or capacity of the battery depends on the concentration and the volume of the redox couples in the electrolytes.[12] Hence, the power and energy or capacity of a flow battery can be designed independently,[13] allowing the power of a flow battery to range from the 100 kW to the 100 MW level and the energy of a flow battery to range from the 100 kWh to the 100 MWh level.[14] Normally, the electrolyte of a flow battery consists of an aqueous solution, which endows the technology with high safety and minimal potential risk of fire or explosion. These advantages of flow battery technologies make such devices very suitable for energy storage applications.

As a representative flow battery technology, the vanadium flow battery (VFB) has long been considered as one of the most mature technologies and is currently at the commercial demonstration stage.[8,15] However, some limitations and challenges, e.g., the relatively high cost[16] and low energy density, still need to be overcome to realize its industrialization. Recently, tremendous efforts have been devoted to exploring and developing novel flow battery technologies with low costs and high energy densities, e.g., zinc-based flow batteries (ZFBs),[17–21] polymer-based flow batteries,[22–24] and quinone-based flow batteries.[25–28] These newly developed flow battery technologies have demonstrated promise for energy storage applications, although most are still in development in the lab.

Dr. Z. Z. Yuan, Dr. Y. B. Yin, C. X. Xie, Prof. H. M. Zhang, Prof. X. F. Li
Division of Energy Storage
Dalian National Laboratory for Clean Energy
Dalian Institute of Chemical Physics
Chinese Academy of Sciences
457 Zhongshan Road, Dalian 116023, P. R. China
E-mail: lixianfeng@dicp.ac.cn
Prof. H. M. Zhang, Prof. X. F. Li
Collaborative Innovation Center of Chemistry for Energy Materials (iChEM)
Dalian 116023, P. R. China
Prof. Y. Yao
Department of Electrical and Computer Engineering and Materials Science and Engineering Program
University of Houston
Houston, TX 77204, USA
The ORCID identification number(s) for the author(s) of this article can be found under https://doi.org/10.1002/adma.201902025.

DOI: 10.1002/adma.201902025

 © 2019 WILEY-VCH Verlag GmbH & Co. KGaA, Weinheim

Based on the form of the redox couples in the anolyte and catholyte, flow batteries can be divided into liquid–liquid flow batteries and hybrid flow batteries. Normally for flow batteries that involve liquid–liquid redox reactions at both positive and negative half-cells, e.g., the vanadium flow battery,[29,30] quinone bromine (ferrocyanide) flow battery,[28,31] and all iron flow battery,[32] the oxidized and reduced active materials for both positive and negative half-cells are stored in independent electrolyte tanks, and pumped into the battery with exterior pumps. The energy and power rating of these systems thus can be flexibly designed,[33] which makes these flow batteries very appropriate for large scale energy storage applications. Different from liquid–liquid flow batteries, the electrochemical reaction at the anode of ZFBs is a plating-stripping process and is normally called a hybrid flow battery.[22] Thus, the characteristic independence of energy and power ratings does not apply to ZFBs because of the limited areal capacity of the zinc anode.

As the negative half-cell of all ZFBs, the zinc anode can be traced back to the early time when primary zinc batteries (e.g., zinc–manganese dioxide batteries,[34] zinc–air batteries[35–37]) were developed; it features the advantages of low cost, abundance in the earth, high capacity, and inherent stabilities in air and aqueous solutions.[20] These intrinsic advantages make ZFBs very suitable for distributed energy storage applications. By coupling the zinc couple with different redox couples, ZFBs have thus been developed into the most diverse class of flow batteries for energy storage applications. Normally, the active material of ZFBs in the negative electrolyte is the Zn^{2+} or $Zn(OH)_4^{2-}$ ion. Zn^{2+} or $Zn(OH)_4^{2-}$ at the cathode is reduced to zinc metal during the charge process, while the redox couple(s) at the anode is oxidized. The electrochemical reactions are reversed during discharge.

Since the 1970s, numerous ZFBs have been proposed and studied, e.g., zinc–bromine flow batteries, zinc–iron flow batteries and zinc–nickel flow batteries as shown in **Figure 1**. The zinc–bromine flow battery, proposed by Lim et al. in 1977,[38] has become one of the most mature technologies among numerous ZFBs currently in existence, although, in 1884, Charles Renard put forward the zinc–chlorine system,[39] where a flow-through chlorine electrode has to be employed since the solubility of chlorine in the electrolyte is limited. Different from the chlorine couple, bromine is highly soluble in the electrolyte after forming a complex with the complexing agent, affording the battery a theoretical specific energy of 428 Wh kg^{-1}.[21] The battery employs $ZnBr_2$ as the active material for both positive and negative half-cells, which avoids contamination issues from both sides. During the charging process, the Br^- in the positive side is oxidized to Br_2, while the Zn^{2+} in the negative side is reduced to zinc metal, endowing the battery with a potential of 1.85 V.[40] After a few decades of development, the zinc–bromine flow battery currently is at the demonstration stage, of which the system has been successfully adapted from the kW to MW scale for various applications.[20] For instance, Ensync Energy installed a 500 kWh zinc–bromine flow battery at Illinois Institute of Technology, USA for microgrid applications,[41] and a 0.5 MW/3 MWh zinc–bromine flow battery system was installed by Vionx Energy (previously Premium Power) in 2016 for peak power capacity applications in Massachusetts, USA.[20] Although great progress has been achieved in zinc–bromine flow batteries, the bromine couple remains confronted with many issues that need to be addressed, e.g., the diffusion of Br_2,[42] and the relatively low kinetics of the bromine couple.[43] Hence, exploring and developing complexing agents with a strong complexation ability, high-performance ion-conducting membranes to suppress Br_2 crossover, and high-activity electrode materials to boost the kinetics of the bromine couple are hot research topics for the zinc–bromine flow battery.

Following the zinc–bromine flow battery, the alkaline zinc–iron flow battery, with substantially lower material costs, was proposed in 1981, where ferro-ferricyanide is employed as the positive active material.[21] Critically different from the zinc–bromine flow battery, the anolyte of the alkaline zinc–iron flow battery is an alkaline zincate electrolyte that is deposited on a

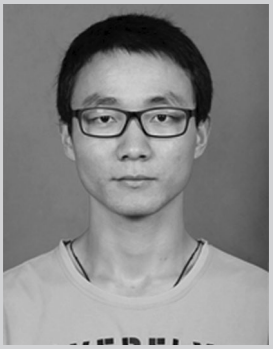

Zhizhang Yuan received his Ph.D. at Dalian Institute of Chemical Physics (DICP), Chinese Academy of Sciences under the supervision of Prof. Xianfeng Li in 2017. Then he was appointed as associate professor at DICP in 2017. His research interests include fundamental and engineering aspects of zinc-based flow batteries for energy storage.

Huamin Zhang is a full professor at Dalian Institute of Chemical Physics (DICP), Chinese Academy of Sciences. He is also CTO of Dalian Rongke Power Co., Ltd and director of the state key lab of flow battery for energy storage. His research interests include the topic of energy and energy storage, fuel cells, flow batteries, and batteries with high specific energy density.

Xianfeng Li received his Ph.D. in polymer chemistry and physics from Jilin University in 2006. Afterward, he joined K.U. Leuven for postdoc research. In 2009, he was appointed as an associate professor in Dalian Institute of Chemical Physics (DICP), Chinese Academy of Sciences. In 2012 he was promoted to full professor. Currently he serves as the head of Energy Storage Division and assistant director of DICP. His research interests focus on electrochemical energy storage.

© 2019 WILEY-VCH Verlag GmbH & Co. KGaA, Weinheim

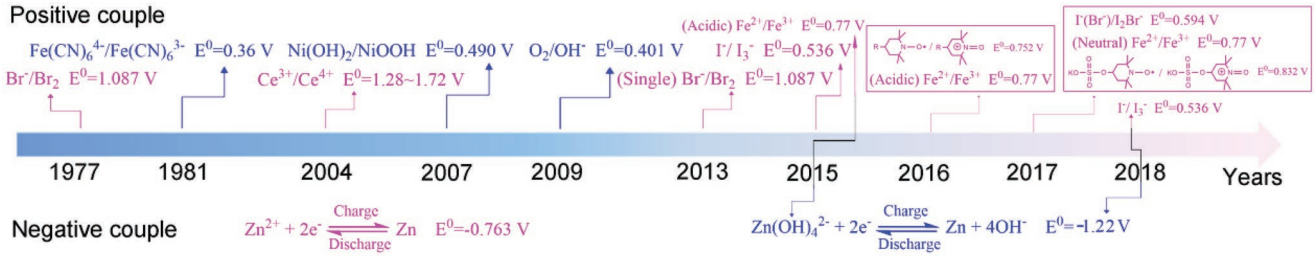

Figure 1. The development history of ZFB technologies.

cadmium-plated iron substrate when the battery is charging. Although the potential of the ferro-ferricyanide couple (0.360 V vs SHE) is significantly lower than that of the bromine couple (1.087 V vs SHE), the potential of the zincate couple ($Zn(OH)_4^{2-}/Zn$) in alkaline media (–1.22 V vs SHE) is also considerably more negative than that of the Zn^{2+}/Zn couple in neutral media (–0.763 V vs SHE), thus affording the battery with a voltage as high as 1.58 V.[20] In addition, this value can reach 1.81 V in a highly concentrated electrolyte, which is attributed to the formation of cationic complexes with the ferro-ferricyanide couple.[21] By employing the $Zn(OH)_4^{2-}/Zn$ pair as the negative redox couple and the nontoxic and cost-effective $Fe(CN)_6^{3-}/Fe(CN)_6^{4-}$ pair as the positive redox couple in alkaline media, a system cost of ≈\$120 kWh^{-1} is projected.[21] In the early stages of its development, the alkaline zinc–iron flow battery employed Nafion as a membrane to prevent the crossover of ferricyanide to the negative half-cell via the charge repulsion mechanism. However, the ion conductivity of the Nafion series in alkaline media is relatively low, which results in the battery working at a relatively low current density (35 mA cm^{-2}) and therefore decreases the power density. Additionally, the use of Nafion membranes in the system would definitely increase the system cost. Another drawback of the alkaline zinc–iron flow battery is that the solubility of ferro-ferricyanide is relatively low (the best reported concentration of this redox couple is 0.4 mol L^{-1}[27,44] in alkaline media), which leads to a battery with a low energy density. This issue also means that the alkaline zinc–iron flow battery system with a defined capacity needs more electrolyte than those systems with active materials of high solubility; therefore, a higher footprint is needed. Although the alkaline zinc–iron flow battery has been proposed since early time, and ViZn Energy (formerly Zinc Air) (http://www.viznenergy.com) is developing an alkaline zinc–iron flow battery module (80 kW/160 kWh) housed in a 20-ft shipping container for grid-scale applications,[10] very little information on the battery chemistry and performance has been disclosed.

Although many different positive redox couples have been put forward to couple with the zinc couple, e.g., the nickel redox couple proposed by Edison in 1901,[45] and the iodine redox couple put forward in 1948,[46] their application in flow battery technologies is long overdue. The zinc–nickel flow battery was proposed by Yang and co-workers in 2007,[47] in which nickel hydroxides serve in the positive electrode and experience a solid-solid electrode reaction. Following this design strategy, only one set of pump and pipeline is necessary (that is, single flow battery), which can endow the battery with a simple structure and cost reduction in comparison with traditional flow batteries. Since the zincate in the supporting electrolyte is chemically inert to the positive redox couple, a membrane-less configuration thus can be adopted, further simplifying the structure and reducing the cost of the battery. When the battery is charged, the zincate in the electrolyte is reduced and deposited onto the negative electrode, of which a zinc plate or a nickel foam is normally used, while in the positive side, the $Ni(OH)_2$ loaded in the nickel foam is oxidized to NiOOH, affording the battery with a potential of up to 1.7 V. Combining the low cost and simple structure of the battery configuration, the single zinc–nickel flow battery is expected to have a low system capital cost that is quite competitive for the application of distributed energy storage. After more than ten years of development, the single zinc–nickel flow battery has been piloted at the dozens-of-kWh scale for energy storage applications, e.g., the 36 kWh battery system installed at the campus of the City College of New York.[48,49] Despite the above advantages and demonstrations, issues associated with the single zinc–nickel flow battery remain. Similar to the case of the bromine redox couple that exhibits relatively low kinetics, the kinetics of the $Ni(OH)_2$/NiOOH couple are inferior as well,[50–53] which results in the battery working at a comparatively low current density and further lowers its power density. In addition to the kinetics of the nickel couple, the area capacity of commercialized 3D porous nickel foams is limited,[54] and a large area of nickel electrode is required to satisfy the needs of the batteries' high capacity. The large area of the nickel electrode in turn leads to heterogeneous electrochemical reactions for both positive and negative half-cells during the charge and discharge, which further aggravate the hydrogen and oxygen evolution side reactions of the battery. Therefore, developing novel battery architectures and designing new kinds of positive electrode materials with a high capacity that can boost the power density or restrain the side reactions of the battery will benefit the commercialization of single zinc–nickel flow batteries.

In addition to the single zinc–nickel flow battery, the single zinc–bromine flow battery has also emerged as an attractive system for stationary energy storage applications. The single zinc–bromine flow battery was first reported by Li and co-workers in 2013 and is currently at the demonstration stage.[55] In 2017, a 5 kW/5 kWh single zinc–bromine flow battery (**Figure 2**a), which is made up of four independent kilowatt class cell stacks, was installed in Shanxi Ankang, China. To further boost the practicability of the single zinc–bromine flow battery, the second-generation of 5 kW/5 kWh single zinc–bromine flow battery system (Figure 2b), with a substantially higher energy density, was assembled successfully. In comparison with the first-generation system, the size of the system is

© 2019 WILEY-VCH Verlag GmbH & Co. KGaA, Weinheim

Figure 2. The demonstrations of single zinc–bromine flow battery. a) The first generation of 5 kW/5 kWh single zinc–bromine flow battery. b) The second generation of 5 kW/5 kWh single zinc–bromine flow battery.

decreased by 70%. Furthermore, the encapsulation of bromine in the electrode avoids the problem with the traditional zinc–bromine flow battery of corrosive Br_2, making the single zinc–bromine flow battery more competitive.

To further improve the energy density of the zinc-based flow battery, some new flow battery systems including zinc–iodine, zinc–(poly)2,2,6,6-tetramethylpiperidinyl-*N*-oxyl, and zinc–iron flow battery systems have been put forward and investigated in detail.[22,56–59] Among which, the zinc–iodine flow battery might be an exception, since the energy density of this kind of battery can reach as high as ≈200 Wh L^{-1}. However, progress in zinc–iodine flow batteries is currently limited by the relatively high cost of ZnI_2. In contrast, the zinc–iron flow battery seems to be more suitable for distributed energy storage applications due to its low cost and relatively high energy density. During the last four years, amphoteric, acidic, neutral and alkaline zinc–iron flow batteries have been reported.[56,60,61] Taking the amphoteric zinc–iron flow battery as an example, the system is based on a double-membrane and triple-electrolyte construction, and the capital cost of this system can be reduced to under \$100 kWh^{-1}.[56] However, as mentioned by the authors, immense challenges to industrial implementation still remain, e.g., the long-term durability and scaling up to large cells and stacks, since the triple-electrolyte construction is relatively complicated. While for the acidic zinc–iron flow battery, although the H_2SO_4 supporting electrolyte in the positive half-cell can effectively address the issue of Fe^{2+}/Fe^{3+} hydrolysis,[60] the protons in the positive electrolyte are likely to migrate to the negative half-cell and react with the zinc metal, further reducing the battery performance. To address the hydrolysis of the Fe^{2+}/Fe^{3+} couple in neutral media, a neutral zinc–iron flow battery has been designed.[61] In this design, a complexing agent is employed to restrain the hydrolysis of the Fe^{2+}/Fe^{3+} couple, thus, affording the battery with improved cycling stability. Since then, several zinc–organic flow batteries, e.g., zinc–TEMPO, zinc–poly (TEMPO) flow battery, have been proposed by Ulrich Schubert and co-workers in succession.[22,62] Nevertheless, these batteries are currently on the lab scale and far from practical applications.

With so many kinds of ZFBs, reviews that focus particularly on advances have been very rare until recently, let alone reviews concentrating on advanced materials for ZFBs. Accordingly, it is urgent to focus on these zinc-based flow battery technologies, and in particular, advanced materials for ZFBs, and make an overview summary. Recently, Shah and co-workers have provided an overview on ZFBs from the perspective of electrochemistry, covering both fundamental information on zinc electrodeposition and recent demonstrations of ZFBs.[20] However, limited information on new chemistries and the fundamental aspects of advanced materials for ZFBs were presented. Furthermore, in light of the latest increase in research activity, especially on advanced materials such as membrane materials, highly active electrode materials and high-concentration electrolytes for ZFBs,[63–65] a complete review of the current status and challenges for ZFB technology has become highly urgent. In this review, we mainly focus on the recent progresses and challenges in terms of advanced materials for ZFBs, e.g., electrode materials, membrane materials and electrolytes. The review will start with a brief classification of ZFBs, followed by a detailed discussion of the common challenges that are associated with ZFBs. Furthermore, the advanced materials for different kinds of ZFBs will be summarized. In particular, the effect of these materials on the battery performance will be discussed in detail. The main objective of this review is to deliver the readers with a timely snapshot of this rapidly developing field.

2. Categories of Zinc-Based Flow Batteries

The history of ZFBs can be traced back to 1884, when the zinc–chlorine system was employed to power an airship.[39] Since then, different types of ZFBs have been developed for potential application in energy storage, and numerous advancements have been achieved. Normally, ZFBs can be divided into two types according to the pH of the supporting electrolyte (**Figure 3**): neutral- or acidic-based ZFBs including zinc–cerium flow battery, zinc–TEMPO flow battery, zinc–poly (TEMPO) flow battery, zinc–bromine or iodine flow battery, single zinc–bromine or iodine flow battery and alkaline-based ZFBs such as zinc–iodine flow battery, single zinc–nickel or air flow battery. Of note is that the zinc–iron flow battery is peculiar, since it can work in a wide range of pH by adopting different varieties of iron couples.[56,59,61,66] The detailed reactions of the zinc anode in different media are as follows

© 2019 WILEY-VCH Verlag GmbH & Co. KGaA, Weinheim

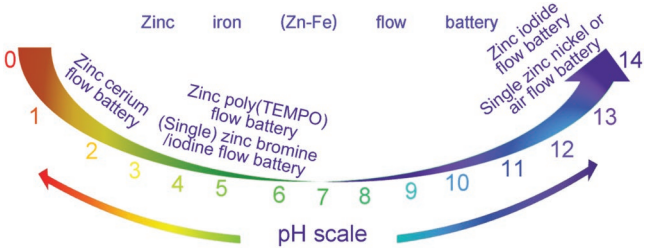

Figure 3. ZFBs in different pH.

$$\text{Neutral or acidulous media}: \quad Zn^{2+} + 2e^- \underset{\text{Discharge}}{\overset{\text{Charge}}{\rightleftharpoons}} Zn \quad E^0 = -0.763\ \text{V} \tag{1}$$

$$\text{Alkaline media}: \quad Zn(OH)_4^{2-} + 2e^- \underset{\text{Discharge}}{\overset{\text{Charge}}{\rightleftharpoons}} Zn + 4OH^- \quad E^0 = -1.22\ \text{V} \tag{2}$$

Clearly, the potential of the zinc couple is relatively negative, especially in alkaline media, which could in turn endow a battery with a high voltage compared to that of other flow batteries (e.g., 1.26 V for vanadium flow battery,[67] 1.02 V for Fe/V flow battery,[68] 1.34 V for all-iron flow battery,[32] 1.20 V for alkaline quinone flow battery[28] and 1.1 V for TEMPO radical-viologen flow battery[24]). Although a higher battery voltage contributes to the higher energy density of a ZFB, this high voltage together with alkaline media bring more critical requirements on the materials' stability. Regardless, the energy density of some ZFBs is still limited by the low solubility of the positive active material, e.g., the TEMPO or poly (TEMPO) couple in neutral media (0.6 M for TEMPO-4-sulfate potassium salt in practical application,[62] 2.39 Ah L^{-1} for poly (TEMPO)[22]), the cerium couple in acidic media (0.8 M in practical application[69]), and the ferrocyanide couple in alkaline media (0.4 M[27,44]). Normally, in alkaline media, the conductivity of the electrolyte is higher than that in neutral media, and the transport of OH^- is significantly faster than that of K^+ or Na^+. The higher electrolyte conductivity together with the faster transport of OH^- can afford alkaline ZFBs a higher operating current density and power density. However, the working current density of a ZFB is closely related to the kinetics of the redox couples, the activity of the electrodes and the ion conductivity of the membranes. Furthermore, in alkaline media, the negative active material is generally prepared by dissolving zinc oxide in a strong base (NaOH, KOH, or LiOH), which means the solubility of the zincate and the conductivity of the negative electrolyte are closely related to the pH of the electrolyte. Meanwhile, a higher alkali concentration brings about the serious issue of zinc metal corrosion,[70–74] resulting in a more serious side reaction of hydrogen evolution. Therefore, advanced materials with different properties are expected to meet the requirements of different ZFBs.

3. The Common Challenges of ZFBs

Regardless, ZFBs have shown very promising prospects for stationary energy storage applications, a portion of which are currently at the demonstration stage such as zinc–bromine and zinc–nickel flow batteries. However, some common issues still exist that all the ZFBs have encountered on account of the similar plating-stripping process of the zinc couple in the negative half-cell, which occurs during charging-discharging of the battery. These issues include zinc dendrite and accumulation,[75–79] a limited areal capacity[80] and a relatively low working current density. In the following, we will briefly introduce how these issues impede the development of ZFB applications.

3.1. Zinc Dendrite and Accumulation

Similar to the case of lithium-based batteries that experience the plating-stripping process, the challenges associated with the zinc couple mainly stem from the zinc dendrite and accumulation (**Figure 4**a,b) that occur when the battery is charging and discharging, and their presence has been identified as one of the most critical issues for ZFBs as well. Since the formation/growth of zinc dendrite, zinc accumulation, and the critical factors influencing zinc dendrite and accumulation in ZFBs have previously been overviewed,[17,20,81,82] we will not overview them further in depth. Actually, the issue of zinc dendrite/accumulation is more serious in alkaline media than in neutral or acidic media, especially at a high working current density. When the battery is charged, the zinc or zincate ions are first plated on the electrode (porous carbon felt or plate electrode), with the formation of zinc metal (dendrite) on the electrode. As the charging proceeds, the zinc or zincate ions in the electrolyte can be plated either in the direction of the electrode or in the direction of the membrane as displayed in Figure 4a,b. Further charging can bring about a short-circuit in the battery since the zinc dendrite can impale the membrane. In the discharge process, the zinc metal (dendrite) intimately contacting the electrode is stripped, while the zinc metal (dendrite) contacting the electrode and the membrane is stripped from both, simultaneously. As long as the zinc metal starts striping from the boundary between the electrode and ion-conducting membrane, the zinc metal may break away from the interface (Figure 4a,b). As a result, the zinc metal remaining in the electrode can be stripped further, while the zinc metal in the membrane cannot be stripped any more, leading to zinc accumulation in the membrane and further raising the resistance of the battery. As the cycling proceeds, this issue will ultimately decrease the reliability of a ZFB. Therefore, obtaining a fundamental understanding of the plating/stripping process at the zinc anode is very important for ZFBs and can help provide effective methods to mitigate or even settle the issue of zinc dendrite and accumulation in ZFBs, e.g., developing advanced membranes with high chemical and mechanical stabilities that can avoid the destruction caused by zinc dendrite, designing novel electrode materials or electrolyte additives that can induce zinc deposition, or designing battery architectures that can essentially allow zinc dendrites form freely.[83–86]

3.2. Limited Areal Capacity

Critically different from liquid–liquid flow batteries, in which both the positive and negative active materials are dissolved in

© 2019 WILEY-VCH Verlag GmbH & Co. KGaA, Weinheim

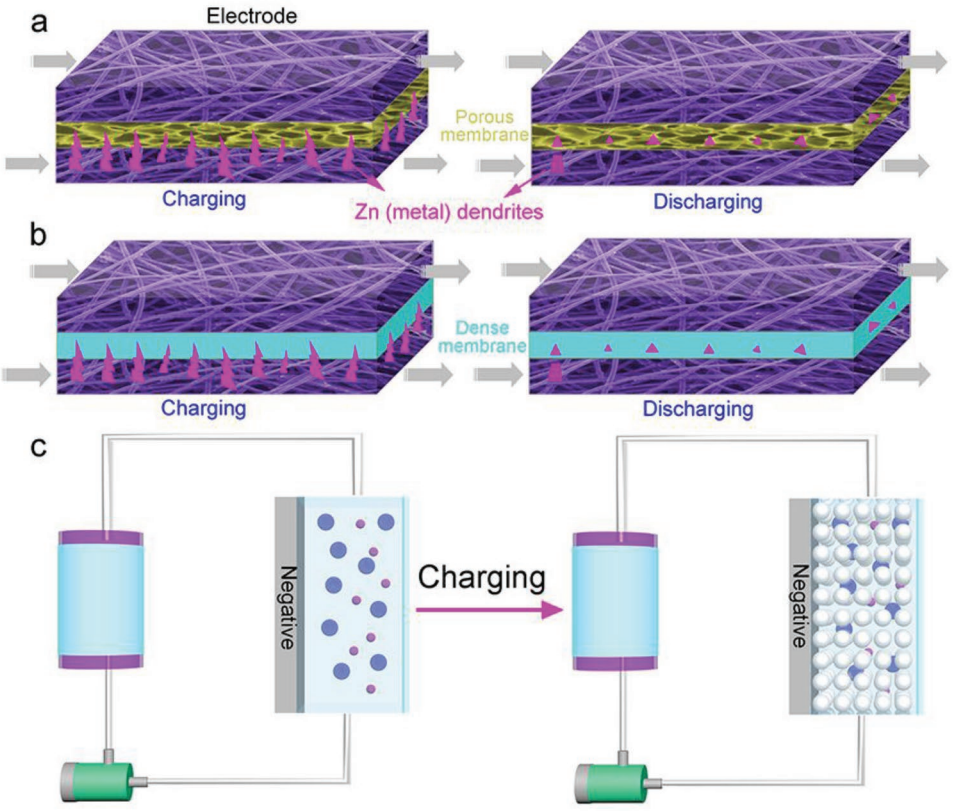

Figure 4. Schematic of the zinc dendrite and accumulation in a ZFB by using different kind of membranes. a) Porous membrane and b) dense membrane. Both porous membrane and dense membrane suffer from the destruction of zinc dendrite. c) Schematic of limited areal capacity of the negative half-cell for a ZFB. The blue balls represent the active material in the negative electrolyte, e.g., Zn^{2+} or $Zn(OH)_4^{2-}$, the purple balls represent the charge-balancing ions, e.g., K^+, Na^+, Cl^- or OH^-, the off-white balls represent zinc metal plated on the electrode.

the electrolytes when the battery is charging and discharging, the electrochemical reaction of the negative half-cell for zinc-based flow batteries is a plating-stripping process when the battery is working. This means that the energy storage capacity and the power rating of a zinc-based flow battery cannot be designed independently as the liquid–liquid flow batteries can be, since the areal capacity of a zinc-based flow battery is limited by the electrode. For ZFBs, porous carbon felt or plate electrodes are usually employed for zinc plating/stripping. As the charging process proceeds, the zinc or zincate ions are continuously reduced to zinc metal on the electrode and ultimately become deposited on the electrode completely (Figure 4c). Once the electrode is completely covered, further plating will no longer take place, and further charging will result in the dramatically increased charge voltage of the battery, consequently leading to an irreversible hydrogen evolution side reaction in the negative half-cell. Using a thicker or highly porous carbon felt electrode for zinc deposition is an effective way to enhance the areal capacity of a ZFB. However, the use of thick porous carbon felt increases the size of the battery (stack) and the cost of the system, simultaneously. Another method is to leave a space between the electrode and the membrane for zinc deposition. Nevertheless, this space will endow the battery with a significantly high polarization. The high polarization in turn causes the battery to work at a relatively low current density, thus reducing the power density. Furthermore, the issue of zinc dendrite/accumulation in the cavity is considerably more serious than the problems associated with ZFBs that adopt porous carbon felt as the electrode, especially in the alkaline media.[59]

3.3. Operating Current Density

The operating current density is one of the key parameters for a flow battery system. A higher working current density normally results in a smaller cell or stack size and further lowers the cost of the system. Typically, the working current density of a flow battery is closely related to the electrochemical activity and the kinetics reversibility of the redox couples at the electrodes, as well as the ion conductivity of the membranes. For liquid–liquid flow battery systems, most of the positive and negative redox couples demonstrate a high reversibility and fast kinetics at their electrode (porous carbon felt), allowing these batteries to work at a high current density (**Table 1**). Hence, compared with the ZFB systems, these liquid–liquid flow battery systems can also deliver a high output power, although their potentials are generally lower than those of ZFBs, as shown in Table 1. By contrast, the ZFB systems are usually operating at a relatively low current density, which is mainly ascribed to the issues associated with the zinc redox couple during the charge–discharge process of the battery. Certainly, the relatively slow kinetics of

© 2019 WILEY-VCH Verlag GmbH & Co. KGaA, Weinheim

Table 1. The comparison of liquid–liquid types of flow battery systems and the zinc-based hybrid flow battery systems.

Liquid–liquid types of flow battery systems	Potential [V]	Working current density [mA cm^{-2}]	Refs.
Polysulfide/iodide	1.05	5-37	[87]
Iron/cadmium	1.17	40–160	[88]
Quinone/bromide	0.858	200–500	[31]
BTMAP-Vi/ BTMAP-Fc	0.748	25–150	[89]
All-Iron	1.34	40	[32]
Quinone/iron	1.20	100	[28]
FcNCl/MV	1.05	40–100	[90]
TEMPTMA/MV	1.40	50–130	[91]
ACA/iron	1.13	100	[44]
MV/4-HO-TEMPO	1.25	20–100	[92]
Polymer-based	1.1	20–80	[24]
FMN/Fe	1.0	5–80	[27]
Fe/V	1.02	50	[68]
$[(NPr)_2TTz]Cl_4$/ N^{Me}-TEMPO	1.44	40–100	[93]
Vanadium flow battery	1.26	10–500	[94–96]
Zinc-based hybrid flow battery systems	**Potential [V]**	**Working current density [mA cm^{-2}]**	**Refs.**
Zinc/bromine	1.85	20–80	[97]
Alkaline zinc/iron	1.58	35–160	[59,98]
Zinc/cerium	2.04–2.48	8–50	[69,99,100]
Single zinc/nickel	1.705	10–300	[47,101]
Single zinc/air	1.621	5–20	[102,103]
Single zinc/bromine	1.85	20–40	[55]
Zinc/polyiodide	1.299	5–180	[64,104]
Amphoteric zinc/ iron	1.99	50–150	[56]
Acidic zinc/iron	1.533	25–30	[60,66]
Zinc/poly(TEMPO)	1.515	1–12	[22]
Zinc/TEMPO	1.595	10–80	[62]
Neutral zinc/iron	1.432	20–80	[61]
Zinc/iodine or bromine	1.357	5–10	[57]
Alkaline zinc/iodide	1.796	20–100	[105]

the positive redox couple also leads to the battery working at a low current density. The main reason is because the zinc dendrite is more serious at a high working current density, which will lead to battery failure from a short-circuit. When the battery is operating at a high current density, the concentration of zinc or zincate ions at the interfacial region of the electrode is exceedingly deficient since the rate of zinc or zincate ions transferring in the bulk solution is significantly lower than their reaction rate at the electrode, leading to a serious concentration polarization. Meanwhile, the diffusion of zinc or zincate ions to the bulge of an electrode is more easily achieved than to the flat surface of an electrode, which makes the plating process of zinc or zincate ions more likely to occur at the bulge, further resulting in the formation of zinc dendrite. Because of grievous zinc dendrite at high working current density, the ZFBs are thereby generally operating under a relatively low current density, especially in practical application. Taking the high potential of ZFB systems into account, seeking effective ways to settle the issue of zinc dendrites that can endow the battery with a high working current density will greatly accelerate the application of ZFB systems.

4. Advanced Materials for Zinc-Based Flow Batteries

As described above, to address the issues and challenges associated with ZFB systems, strategies for developing advanced materials (**Figure 5**) are crucial since the key materials of a ZFB ultimately determine the battery performance. Recently, the advanced materials of ZFBs have attracted increasing attention, including the membranes, electrodes and electrolytes, which has not only greatly boosted these batteries' development but also promoted the development of new ZFB systems. Owing to the diversity of ZFB systems, the advanced materials applied to these batteries are also different from the perspective of the materials' structure, with an aim to accelerate the batteries' development. For instance, the early electrodes used for the ZFB system included carbon plastic or metal-plated substrate electrodes.[21] However, these kinds of electrodes introduce a series of problems for ZFBs as well. For instance, the poor electrochemical activity of the electrodes toward redox couples results in a battery working at a relatively low current density, and the issues associated with zinc dendrite/accumulation at these electrodes is substantially more prominent. In response, with the development of technology and the high requirements of ZFBs for electrodes, increasingly advanced electrode materials with rich structures and a high performance have been developed in succession.[63,106–111] On the other hand, the early membranes applied to the batteries were very limited, and commercialized microporous polyolefin or Nafion membranes were widely used.[8,21,22,57,98,112] As an increasing number of novel redox couples have been discovered and coupled with the zinc redox couple, the limitation of these commercialized membranes has appeared. Moreover, the high cost of the Nafion series of membranes has hampered their widespread application, as well. Thus, aiming to promote the development of ZFBs, membranes with novel structures have been designed and reported in different systems. Combined with the advanced electrode materials and membrane materials, the corresponding electrolytes that include supporting electrolytes and additives have been rapidly developed as well, which has greatly facilitated the development of ZFBs. Therefore, in the following section, we will emphasize the scientific understandings of the fundamental design of the advanced materials' architecture in relation to the performance of batteries and present the remaining challenges as well as possible research directions for future development.

© 2019 WILEY-VCH Verlag GmbH & Co. KGaA, Weinheim

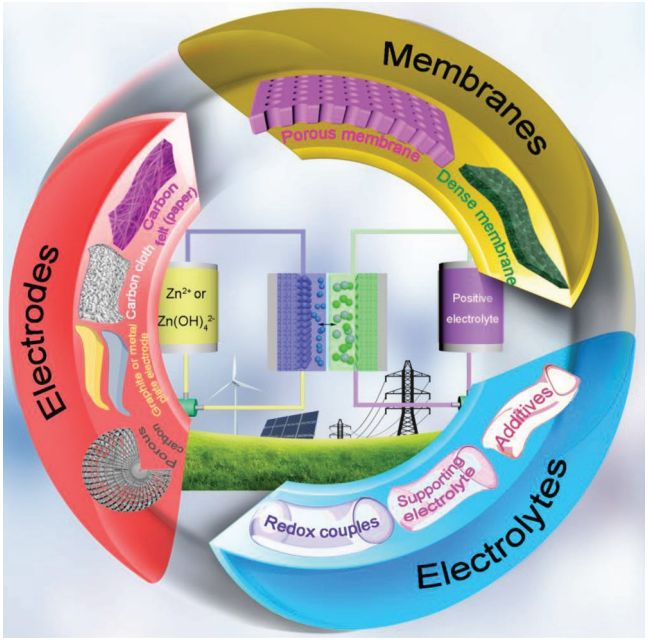

Figure 5. Advanced membrane, electrode and electrolyte materials for ZFBs.

4.1. Membranes

An ion-conducting membrane in a ZFB plays a vital role in isolating the positive and negative electrolytes while conducting the charge-balancing ions to complete the internal circuit.[113] The optimal ion-conducting membrane for a ZFB should meet the requirement of high ion conductivity to minimize the resistance of the battery, high ion selectivity to avoid self-discharge, excellent chemical stability to resist the highly corrosive positive redox couple and high mechanical stability to protect the membrane from the damage due to zinc dendrites. Thus, the properties of an ion-conducting membrane will ultimately determine the performance and reliability of a ZFB. The design of membrane materials with unique distinctions that can endow the battery with a high performance and reliability is thus very important for ZFB systems.

4.1.1. Membranes for Neutral or Acidic ZFBs

Currently, the categories of membrane materials applied in neutral and acidic ZFBs are very limited, of which the commercialized Nafion series of ion exchange membranes and porous Daramic membranes are the most widely used (**Figure 6**) on account of their ultrahigh stability and availability. Membranes with novel structures from the view of both materials and morphology have rarely been reported. In addition to the above membranes, other kinds of membranes are employed as well, however, they only account for a minority of ZFB systems, e.g., dialysis membranes for the zinc–poly (TEMPO) flow battery,[22,114] the HZ 115 ion exchange membrane for the acidic zinc–iron flow battery[60] and the fumasep F-930-RFD cation exchange membrane for the zinc–TEMPO flow battery.[62] Actually, synthesizing novel materials or adopting membranes from

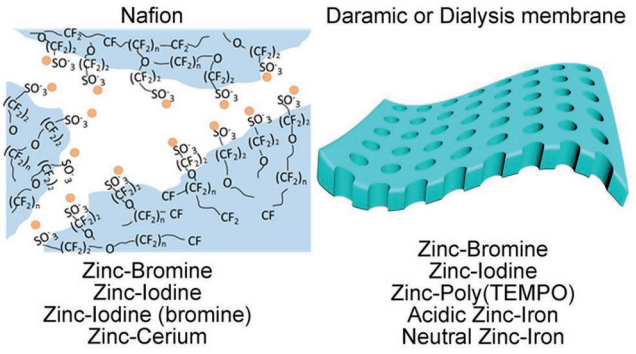

Figure 6. Membranes applied in neutral and acidulous ZFB systems.

other battery technologies including fuel cells, vanadium flow batteries and water treatment systems is very challenging since the majority of ZFB systems involve a strongly oxidizing and high potential environment, especially zinc–halogen flow batteries and zinc–cerium flow batteries.

Therefore, membrane modification based on Nafion or Daramic is the mainstream for these ZFB systems. For instance, the zinc–bromine flow battery usually demonstrates a high energy density and cost efficiency. However, porous polyethylene membranes such as SF-600 or porous polypropylene (PP) membranes (Daramic) that are widely applied in the zinc–bromine flow battery normally suffer from a relatively high Br_2 crossover,[115] which leads to battery self-discharge and an irreversible capacity decay.[116] To prevent Br_2 crossover through the membrane, Kim and co-workers presented an ultrathin Nafion-filled PP membrane for the zinc–bromine flow battery (**Figure 7**a).[115] By casting a 10 wt% Nafion solution onto a porous PP membrane (Figure 7b,d), the pores become filled with the Nafion ionomer, as displayed in Figure 7c,e. After impregnating with the Nafion ionomer, the thickness of Nafion/PP (Figure 7e) is thinner than that of the pristine PP membrane (Figure 7d) because the pores in the PP membrane are compacted during the drying process. As expected, the Nafion/PP composite membrane with a 16 µm Nafion layer shows a Br_2 diffusivity of 7.53×10^{-9} cm^2 min^{-1}, which is two orders of magnitude lower than that of the SF-600 membrane (2.67×10^{-7} cm^2 min^{-1}) with a thickness of 600 µm. Due to the ultrathin thickness, the ASR of the Nafion/PP composite membrane (3.12 Ω cm^2) is lower than that of the SF-600 membrane (4.2 Ω cm^2), affording the zinc–bromine flow battery with a lower charging voltage and a higher discharging voltage (Figure 7f). Nevertheless, whether the Br_2 blocking ability of the Nafion/PP composite membrane originates from the Nafion or the compacting of the pores of PP during drying process still needs further verification.

Due to the high selectivity of halogen, the Nafion series or perfluorinated ion exchange membranes are widely employed since they can endow a battery with a high coulombic efficiency (CE) and low self-discharge. In addition to the (single) zinc–bromine flow battery,[55] the first reported ambipolar zinc–polyiodide flow battery system proposed by Wang and co-workers[104] also adopts Nafion (Nafion 115) as the membrane, which delivers a CE of over 99%, even at a current density of 5 mA cm^{-2}. However, the voltage efficiency (VE) of the battery with a Nafion 115 membrane is relatively low because of the

© 2019 WILEY-VCH Verlag GmbH & Co. KGaA, Weinheim

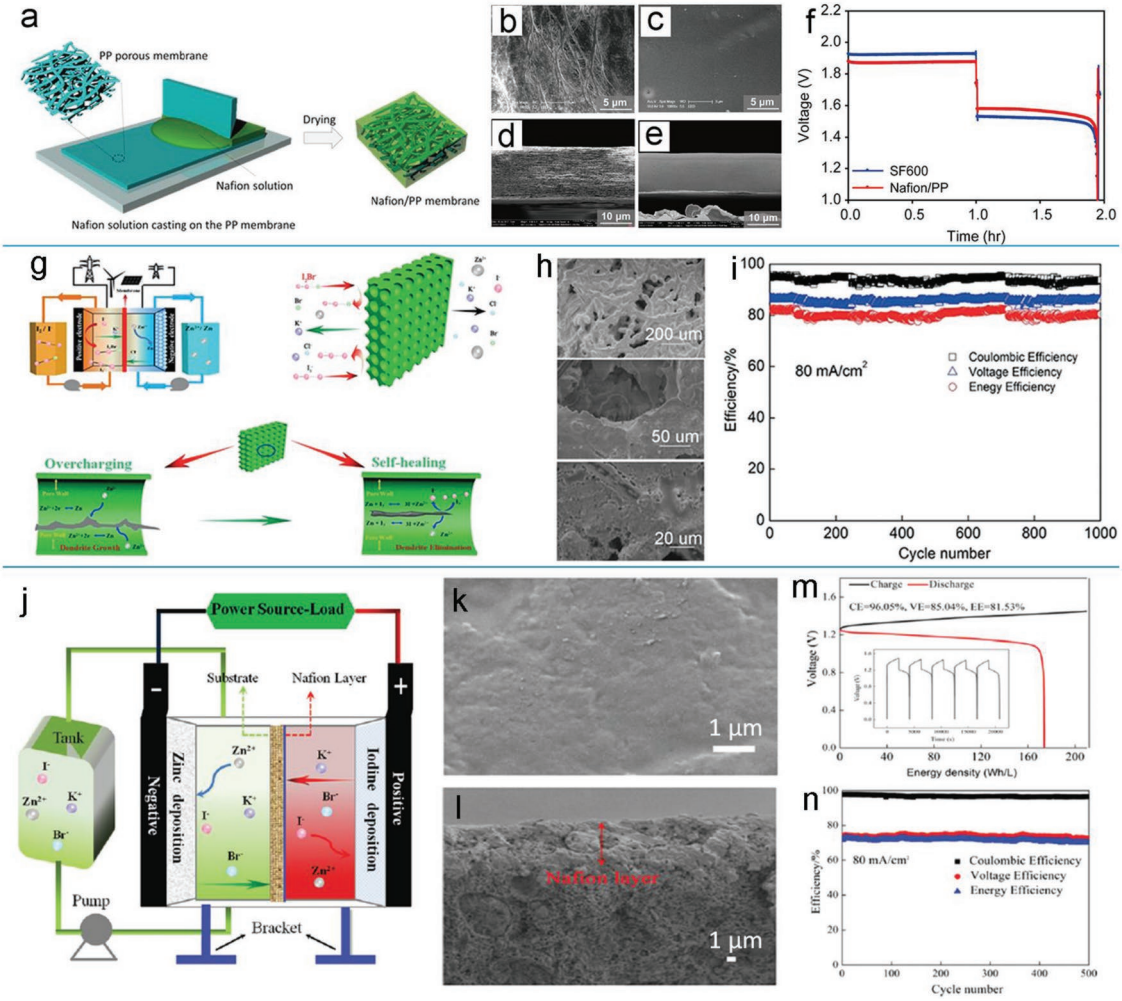

Figure 7. Membranes for zinc–bromine and (single) zinc–iodine flow batteries. a) Schematic of Nafion-filled porous membrane (Nafion/PP) for zinc–bromine flow battery. b) Surface and d) cross-section images of the porous PP membrane. c) Surface and e) cross-section images of the Nafion/PP membrane. f) The charge and discharge curves of the zinc–bromine flow battery assembled with a SF600 and a Nfion/PP membrane. Reproduced under the terms of the Creative Commons Attribution 4.0 International License.[115] Copyright 2017, The Authors, Springer Nature. g) Schematic of overcharging and self-healing process of the zinc–iodine flow battery using a porous polyolefin membrane. h) The morphology of the zinc deposition with different magnifications at the current density of 80 mA cm^{-2}. i) Cycling performance of the zinc–iodine flow battery with a 6 M electrolyte. Reproduced with permission.[64] Copyright 2018, Wiley-VCH Verlag GmbH & Co. KGaA, Weinheim. j) The schematic of a single zinc–iodine flow battery. k) Surface and l) cross-section morphologies of a Nafion coated porous polyolefin membrane. m) The charge–discharge curve of a single zinc–iodine flow battery operating at 40 mA cm^{-2} with a 6 M electrolyte. n) The cycling performance of a single zinc–iodine flow battery with 6 M electrolyte at 80 mA cm^{-2}. Reproduced with permission.[58] Copyright 2019, The Royal Society of Chemistry.

high membrane resistance, which in turn leads to the battery working at a relatively low current density (20 mA cm^{-2}), together with a relatively low cycling stability (less than 40 cycles at 10 mA cm^{-2}). Regardless, the zinc–iodine flow battery still demonstrates promise for use in energy storage applications on account of its high energy density as well as its benign nature being free from strong acids and other corrosive chemicals. To advance the development of the zinc–iodine flow battery, Li and co-workers recently reported a zinc–iodine flow battery with a very long cycle life, high energy and high power densities, and a self-healing behavior by using a polyolefin porous membrane for the first time (Figure 7g),[64] and these properties are attributed to the low membrane resistance compared to that of the Nafion 115 membrane.[55] The porous polyolefin membrane can on one hand reduce the ohmic resistance of the battery, which affords the battery with a high performance, while on the other hand, the component addresses the issue of zinc dendrite in the battery, affording the battery with a very long cycle life. During the charging of the battery, the pores of the membrane are filled with a solution containing oxidized I_3^- that can react with zinc metal when the battery is overcharging or the zinc dendrites are piercing into the membrane as shown in Figure 7g. The reacting with zinc dendrites enables the battery to self-recover from microshort-circuiting and further affords the battery with a very long cycle life. Therefore, even working at a current density of 80 mA cm^{-2}, no apparent zinc dendrites can be found (Figure 7h), and thus, the battery exhibited more than 1000 charge/discharge

© 2019 WILEY-VCH Verlag GmbH & Co. KGaA, Weinheim

cycles (over 3 months) without a clear efficiency drop (Figure 7i). In addition to the above advantages, the pore structure of the polyolefin porous membrane can also endow the membrane with a high ion conductivity. Even working at a current density of 80 mA cm^{-2}, the zinc–iodine flow battery can deliver a VE of ≈80%. Nevertheless, this self-healing behavior, dendrite-free environment and long cycle life are achieved with the sacrifice of a reduced CE, resulting from the chemical reaction between zinc metal and I_3^-. Overall, the zinc–iodine flow battery with a low-cost porous polyolefin membrane can be regarded as a very promising option for energy storage application, which is confirmed by a kW stack with more than 300 cycles at a current density of 80 mA cm^{-2}.[64]

To further improve the membrane selectivity and address the issue of self-discharge, a single zinc–iodine flow battery was proposed (Figure 7j) to include a composite membrane, which consists of a thin Nafion selective layer and a porous polyolefin substrate (Figure 7k,l).[58] The ultrathin layer of Nafion (7 µm) on the porous polyolefin substrate can effectively hinder the crossover of I_3^-/I_2, which endows the battery with a CE of above 96% and a VE of above 85% at a current density of 40 mA cm^{-2} together with a discharge energy density of above 160 Wh L^{-1} (Figure 7m). Even working at a current density as low as 20 mA cm^{-2}, the CE of a single zinc–iodine flow battery assembled with a Nafion-coated porous polyolefin membrane can reach as high as 92%, which is 18% higher than that afforded by the pristine porous polyolefin substrate. Most importantly, a single zinc–iodine flow battery assembled with the composite membrane can provide a stable performance over 500 cycles without an apparent efficiency decay at a current density of 80 mA cm^{-2} (Figure 7n), further confirming the high selectivity and stability of the as-prepared composite membrane.

Another successful example introduced a polybenzimidazole (PBI) porous membrane into a neutral zinc–iron flow battery as shown in **Figure 8**a.[61] A PBI membrane with a sponge-like pore structure was created by the typical vapor-induced phase inversion method (Figure 8b–e). The membrane morphology, including the pores' connectivity, can be well-tuned by altering the membrane formation conditions, e.g., the concentration of the cast solution, the temperature and humidity, which has already been well studied for vanadium flow battery applications.[8,15] In combination with optimized electrolytes, where the complexing agent glycine is used to suppress the hydrolysis of Fe^{2+}/Fe^{3+}, the neutral zinc–iron flow battery with a porous PBI membrane delivers a stable performance for more than 100 cycles at a current density of 40 mA cm^{-2}, along with a CE of above 97% and an EE of above 84% (Figure 8f). As a reference, the performance of the neutral zinc–iron flow battery with a Nafion 115 membrane was also investigated. Unfortunately, the energy efficiency (EE) of the battery significantly decreases within 100 cycles under the same conditions (Figure 8i), and after cycling, the membrane (Figure 8g) exhibits serious fouling from the Fe^{3+} (Figure 8h), which in turn results in an increased polarization of the battery. Judging from the results, the cation exchange membranes are not very suitable for this neutral zinc–iron flow battery since Fe^{2+}/Fe^{3+} can exchange with the cations from the membranes. Regardless, complexing agents with a higher complexing ability to restrain the hydrolysis and crossover of Fe^{2+}/Fe^{3+} need to be further explored to improve the reliability of the zinc–iron flow battery. In summary, innovative material and structure design has afforded an excellent membrane that delivers significantly better performance than that of the widely used Nafion 115 membrane over wide current density and temperature ranges in terms of both selectivity and conductivity, at the benefit of a substantial cost reduction.

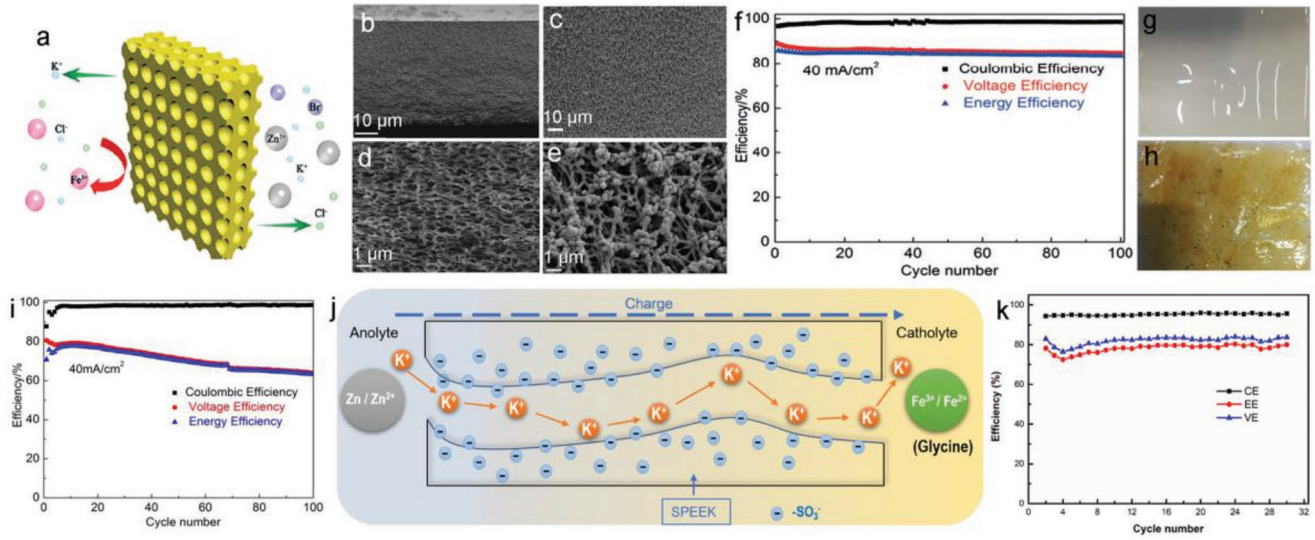

Figure 8. Membranes for zinc–iron flow battery. a) Schematic of porous polybenzimidazole (PBI) membrane. b) Cross-section morphology and d) magnified cross-section morphology of the PBI porous membrane. c) Surface morphology and e) magnified surface morphology of the PBI porous membrane. f) Cycling performance of a zinc–iron flow battery with a porous PBI membrane at 40 mA cm^{-2}. g) The prototype of a Nafion 115 membrane. h) The prototype of a Nafion 115 membrane after cycling test. Reproduced with permission.[61] Copyright 2017, Wiley-VCH Verlag GmbH & Co. KGaA, Weinheim. i) Cycling performance of a zinc–iron flow battery with a Nafion 115 membrane at 40 mA cm^{-2}. j) Schematic illustration of a SPEEK-K membrane in a zinc–iron flow battery. k) Cycling performance of a zinc–iron flow battery with a SPEEK-K membrane at 40 mA cm^{-2}. Reproduced with permission.[117] Copyright 2018, Elsevier B.V.

© 2019 WILEY-VCH Verlag GmbH & Co. KGaA, Weinheim

To further verify the application of cation exchange membranes in the neutral zinc–iron flow battery, Cheng et al. reported a low-cost K^+-formed sulfonated poly(ether ether ketone) (SPEEK-K) membrane (Figure 8j).[117] The battery with the SPEEK-K membrane shows a CE of over 95% and an EE of over 78% at a current density of 40 mA cm^{-2}, demonstrating a slightly better performance than that of the battery with a Nafion 117 membrane. Nevertheless, the cycling performance of the battery with the SPEEK-K membrane needs to be further investigated (≈30 cycles, Figure 8k).

4.1.2. Membranes for Alkaline Zinc-Based Flow Batteries

Compared with the membranes used in neutral and acidic media, the requirements for membranes applied in alkaline media are far more rigorous since an alkaline medium is more aggressive—especially toward anion exchange membranes, having already been proven as unstable in alkaline fuel cells.[8,118–120] Currently, perfluorinated ion exchange membranes are still the most used membranes in alkaline-based flow batteries.[8] However, their performance and voltage efficiency in particular are relatively poor, and the mechanism and transport behavior of ions through these membranes are unclear.[121] Recently, we investigated the physical and electrochemical behaviors of a Nafion membrane in different alkaline solutions by combining experimental with computational strategies.[121] Taking the alkaline zinc–iron flow battery as an example, we found that a battery assembled with a Nafion 212 membrane shows a significantly higher VE when employing NaOH as the supporting electrolyte (≈86% at 80 mA cm^{-2}) than does a battery using KOH as the supporting electrolyte (≈79% at 80 mA cm^{-2}) (**Figure 9**a). Further studies indicated that the Nafion membrane possesses a higher degree of phase separation and larger cluster radius in the NaOH solution than it does in the KOH solution (Figure 9b), endowing the Nafion membrane with a higher ion conductivity in the NaOH solution. In addition, the binding energy between Na^+ and the $-SO_3^-$ in Nafion is relatively higher than that of the binding energy between K^+ and the $-SO_3^-$ in Nafion, as calculated by DFT (Figure 9c). The higher binding energy means faster adsorption and desorption rates between the cations and the $-SO_3^-$ in Nafion, which induces a faster transfer rate of Na^+ through the Nafion membrane in the NaOH supporting electrolyte. Taken together, when using NaOH as the supporting electrolyte, the alkaline zinc–iron flow battery with a Nafion membrane exhibits a higher performance than that of the battery using KOH as the supporting electrolyte tested under the

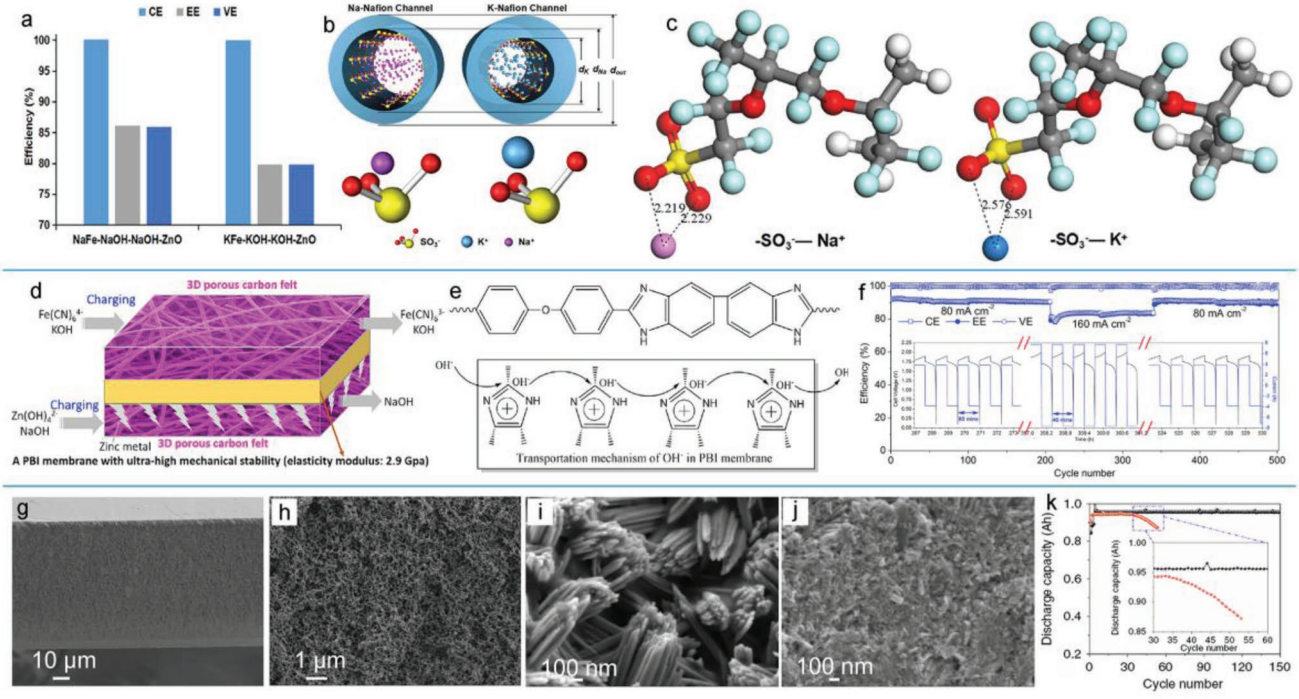

Figure 9. Membranes for alkaline zinc–iron flow battery. a) The battery performance of the alkaline zinc–iron flow battery with a Nafion 212 membrane using different kind of electrolyte at the current density of 80 mA cm^{-2}. b) Scheme of ion cluster size of Nafion 212 in NaOH and KOH solutions. c) DFT calculation of the interaction between $-SO_3^-$ in Nafion 212 and the cations (K^+ or Na^+) in the electrolyte. Reproduced with permission.[121] Copyright 2018, Elsevier B.V. d) Schematic of a self-made PBI membrane with ultrahigh mechanical stability for an alkaline zinc–iron flow battery. e) Transportation mechanism of OH^- through a PBI membrane. f) The cycling performance of an alkaline zinc–iron flow battery using a PBI membrane. Reproduced with permission.[59] Copyright 2018, Elsevier. g) Cross-sectional and h) magnified cross-sectional morphologies of a negatively charged nanoporous membrane (P20). i) SEM image of zinc metal (dendrite) at the end of 53rd charge of the battery with a P0 membrane. j) SEM image of zinc metal at the end of 183rd charge of the battery with a P20 membrane. k) Discharge capacity of the alkaline zinc–iron flow batteries with a negatively charged (P20) and an uncharged (P0) nanoporous membrane. Reproduced under the terms of the Creative Commons Attribution 4.0 International License.[65] Copyright 2018, The Authors, Springer Nature.

© 2019 WILEY-VCH Verlag GmbH & Co. KGaA, Weinheim

same condition. Based on these results, the currently reported as well as the forthcoming alkaline-based flow batteries with a Nafion membrane are expected to deliver an improved performance through adopting NaOH as the supporting electrolyte.

Although we have found the application of Nafion series ion exchange membranes in some ZFB systems, the relatively high cost and low performance will restrict their further application. Therefore, developing new types of membranes with a high performance as well as a low cost for ZFBs is desperately needed. For example, a homemade, cost-effective PBI membrane was recently introduced into the alkaline zinc–iron flow battery (Figure 9d) by us.[59] The ultrahigh mechanical stability of the PBI membrane can effectively resist zinc dendrite even at a very high current density (160 mA cm^{-2}) during the metal plating, thus affording the battery with a long cycle performance as well as a high power density. The high ion conductivity of the membrane can be realized by the base-doped heterocyclic rings in the PBI polymer chain (Figure 9e), which in turn endows the battery with a high power density. Considering the excellent alkali stability, PBI is well suited for alkaline zinc-based flow battery applications. After treating the membrane with a 3 mol L^{-1} sodium hydroxide solution at 30 °C for more than 1 month, an alkaline zinc–iron flow battery assembled with a PBI membrane can still deliver a stable performance for more than 500 cycles with a current density ranging from 80 to 160 mA cm^{-2} (Figure 9f), demonstrating the excellent stability of the PBI membrane in the alkaline zinc–iron flow battery media. The battery exhibited an EE of above 80%, even at a high working current density of 160 mA cm^{-2}, which is by far the highest current density ever reported among the ZFBs systems. In addition to the excellent battery performance, the PBI membrane can resist zinc dendrite growth very well because of its ultrahigh mechanical stability (elastic modulus: 2.9 GPa). Thus, even working with current densities ranging from 60 to 160 mA cm^{-2}, the battery demonstrates a very stable performance. Taken together, the PBI membrane with ultrahigh mechanical stability and high ionic conductivity is very promising for alkaline ZFBs.

Apart from dense membranes such as PBI, porous membranes are another option for alkaline ZFBs.[65] In contrast to the commercialized porous polyolefin membrane applied in (single) zinc–iodine (bromine) flow batteries, the design of this membrane is to inhibit the zinc dendrites via controlling the dendrite growth direction by changing the charge properties of the membrane. The porous membrane is made up of poly (ether sulfone) (PES) and negatively charged sulfonated poly (ether ether ketone) (SPEEK) (Figure 9g,h). For the alkaline zinc–iron flow battery, the active material in the negative electrolyte exists in the form of $Zn(OH)_4^{2-}$. As shown in Figure 4a,b, when the battery is charging, the $Zn(OH)_4^{2-}$ can be plated in either the electrode direction or the membrane direction. By employing negatively charged PES/SPEEK (P20) as the membrane, the zinc metal plated in the membrane direction can be prohibited because of the charge repulsion between the negatively charged $Zn(OH)_4^{2-}$ and the negatively charged surface and pore walls of the nanoporous membrane, thus, avoiding the membrane from being pierced and further affording a dendrite-free alkaline zinc–iron flow battery with long cycle life (Figure 9k). After the cycling test, the deposited zinc of the battery with a conventional nanoporous membrane demonstrates obvious zinc dendrites with a needle-shaped formation on the electrode (Figure 9i), whereas a smooth zinc morphology can be found for the battery with a negatively charged P20 membrane (Figure 9j), indicating that the plating of $Zn(OH)_4^{2-}$ can be easily switched from the membrane direction to the electrode direction through the charge repulsion mechanism. Benefiting from the negative charges on the porous membrane, an alkaline zinc–iron flow battery can be operated at a high current density of 160 mA cm^{-2}. More importantly, the areal capacity of an alkaline zinc–iron flow battery with a P20 membrane can reach up to 154 mAh cm^{-2}, which is the highest value among recently reported zinc-based flow batteries. This strategy can offer another possible solution to address the issue of zinc dendrite/accumulation and can greatly improve the areal capacity for alkaline zinc-based batteries.

4.2. Electrode

The electrode is another important component of the ZFB; it provides active sites for redox reactions, but the electrode itself does not participate in the reactions.[122,123] The physicochemical properties of the electrode have significant impact on the battery performance. For example, the electrocatalytic activity and reversibility of the electrode with respect to the redox couples normally determine the electrochemical polarization of a battery, the electrical conductivity and thickness of the electrode determine the ohmic polarization of a battery, and the pore structure and hydrophilicity of the electrode determine the concentration polarization of a battery.[63,103,124–131] Therefore, the desired electrode material for zinc-based flow batteries should meet the requirements of a high electrocatalytic activity and reversibility for redox couples, high electrical conductivity, and the appropriate hydrophilicity and pore structure. Furthermore, excellent mechanical and (electro)chemical stabilities to guarantee a long cycle life and a low cost are also indispensable characteristics for the electrode materials of ZFBs.

Currently, the electrodes can be mainly divided into four types, namely, metal plate electrodes, carbon-based plate electrodes, porous metal electrodes, and porous carbon-based electrodes.[21,71,132–138] Among these electrodes, plate electrodes are usually employed for zinc plating/stripping since the porosity of porous electrodes is limited, leading to the restricted areal capacity of a ZFB. Indeed, the areal capacity of a ZFB with a plate electrode is restricted as well since the space between the electrode and the membrane is also constrained. Additionally, the electrocatalytic activity of the plate electrodes toward redox couples is relatively low, and the plate structure of the electrodes results in a high concentration polarization, which in turn leads to the battery working at a low current density. Accordingly, the porous electrodes, and porous carbon electrodes in particular,[63,97,139] are increasingly receiving attention on account of their high electrocatalytic activity, high stability, and wide operation potential range.[123]

4.2.1. Electrode for Neutral or Acidic ZFBs

Electrode for Positive Half-Cells: Currently, porous carbon materials such as carbon felt, carbon cloth and carbon paper are the

© 2019 WILEY-VCH Verlag GmbH & Co. KGaA, Weinheim

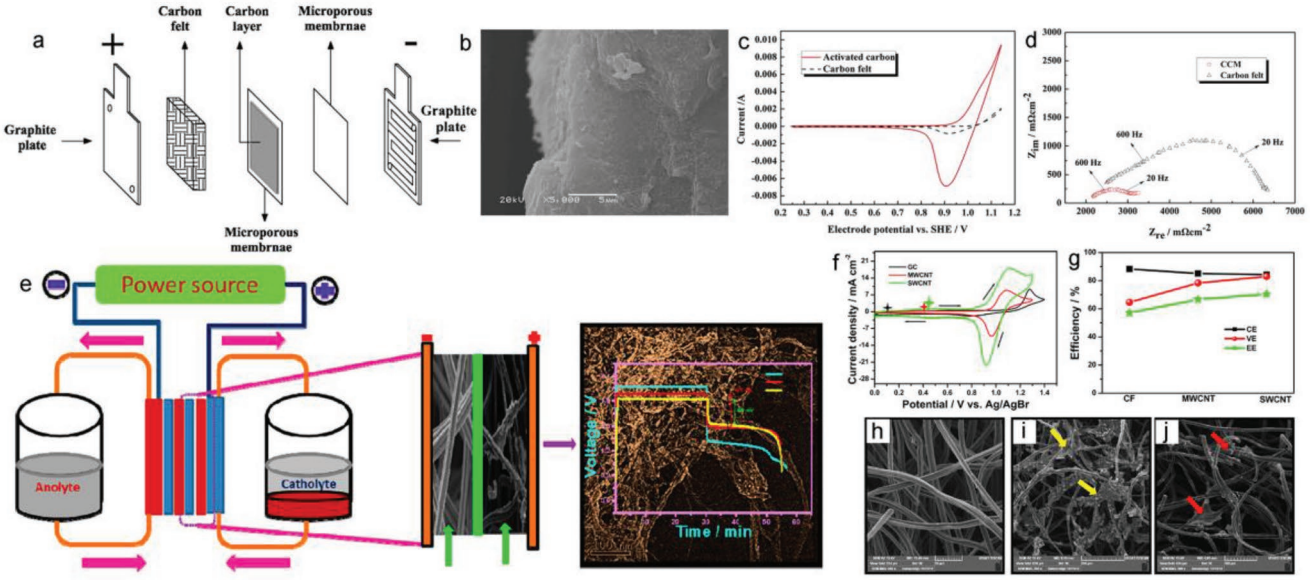

Figure 10. Electrodes for zinc–bromine flow battery. a) Schematic of zinc–bromine flow battery using a carbon coated membrane (CCM). b) Cross-section morphology of carbon coated membrane. c) Cyclic voltammetry of the activated carbon and carbon felt with a scan rate of 20 mV s^{-1} at 25 °C. d) Impedance spectra of the zinc–bromine flow battery by using CCM and carbon felt at the open circuit voltage. Reproduced with permission.[140] Copyright 2012, Elsevier B.V. e) Zinc–bromine flow battery using CNT-anchored carbon felt (CF) as bromine electrode. f) Cyclic voltammograms of single-walled carbon nanotube (SWCNT) and multiwalled carbon nanotube (MWCNT)-modified electrodes and glassy carbon electrode (GCE) at 20 mV s^{-1} in 0.05 M $ZnBr_2$ containing 1 M $HClO_4$. g) The efficiency of the zinc–bromine flow battery with various electrodes. SEM images of h) carbon felt, i) SWCNT modified CF, and j) MWCNT modified CF. Arrow marks show the CNT anchored on CF. Reproduced with permission.[109] Copyright 2014, American Chemical Society.

most widely used electrodes for ZFBs. However, the electrocatalytic activity of these electrodes toward some redox couples, such as the bromine redox couple, is relatively low. Given that the electrocatalytic activity closely depends on the electrode's structure, surface chemistry, surface area, etc., varied approaches have been employed to optimize porous carbon electrodes. For instance, in 2013, Zhang et al. proposed a carbon modified Daramic membrane for use in the zinc–bromine flow battery (**Figure 10**a).[140] By spraying activated carbon ink onto the surface of the microporous membrane (Figure 10b), the internal resistance of the battery can be decreased significantly. Since activated carbon features a high specific surface area and strong adsorption ability, it delivers a higher electrochemical activity toward the bromine couple than the carbon felt does (Figure 10c). Thus, the authors believed that the electrochemical reaction sites are concentrated in the activated carbon layer. In addition, the ionic transport distance is shortened since the activated carbon layer is very close to the membrane, which further lowers the internal resistance of the battery as shown by the impedance spectra in Figure 10d.

In addition to activated carbon, noble metal, noble metal oxide (Pt and IrO_2) and commercial carbon nanotubes were also found to exhibit a high electrocatalytic activity toward the bromine couple.[97,107,109] To better reveal the electrocatalytic effect of carbon nanotubes on the electrochemical behavior of the bromine couple, Pillai et al. conducted exhaustive research on the kinetics of the bromine couple with carbon nanotube and modified carbon felt electrodes and further compared the results with those of single-walled carbon nanotube (SWCNT)- and multiwalled carbon nanotube (MWCNT)-modified carbon felt electrodes (Figure 10e).[109] The results demonstrated (Figure 10f) that the SWCNT electrode shows the best electrocatalytic activity toward the bromine couple due to the large, available basal plane of SWCNTs. By contrast, the MWCNT electrode exhibits a higher reversibility for the bromine couple than does the SWCNT electrode, possibly originating from the additional edge and plane active sites in MWCNTs. Because of the improved electrocatalytic activity, the zinc–bromine flow battery with SWCNT-anchored carbon felt (CF) as the bromine electrode delivers the highest VE at 20 mA cm^{-2}, whereas the battery with pristine CF shows the lowest VE on account of its sluggish electrocatalytic activity toward the bromine couple (Figure 10g). The battery with the SWCNT-anchored carbon felt (CF) as the bromine electrode can indeed afford a higher VE than that of the battery with the MWCNT-anchored carbon felt (CF) as the bromine electrode (Figure 10g). However, the anchored stability of the SWCNTs on the surface of CF is higher than that of MWCNTs, which affords a higher density of SWCNTs on the surface of CF (Figure 10h–i). The higher density of SWCNTs on the surface of CF can also contribute to a higher VE of the battery.

Although the activated carbon and the CNTs have been shown to demonstrate high electrocatalytic activity toward the bromine couple and to further enhance the zinc–bromine flow battery by working at a relatively high current density (normally 40 mA cm^{-2}), the battery performance at higher working current densities still cannot meet the practical requirements. In addition, the relatively high cost of CNTs hinders their further application. The research and development of high-electrocatalytic-activity electrode materials remain urgently needed. Therefore, many efforts have been carried out to fabricate electrode materials for the zinc–bromine flow battery. For example, Zhang

© 2019 WILEY-VCH Verlag GmbH & Co. KGaA, Weinheim

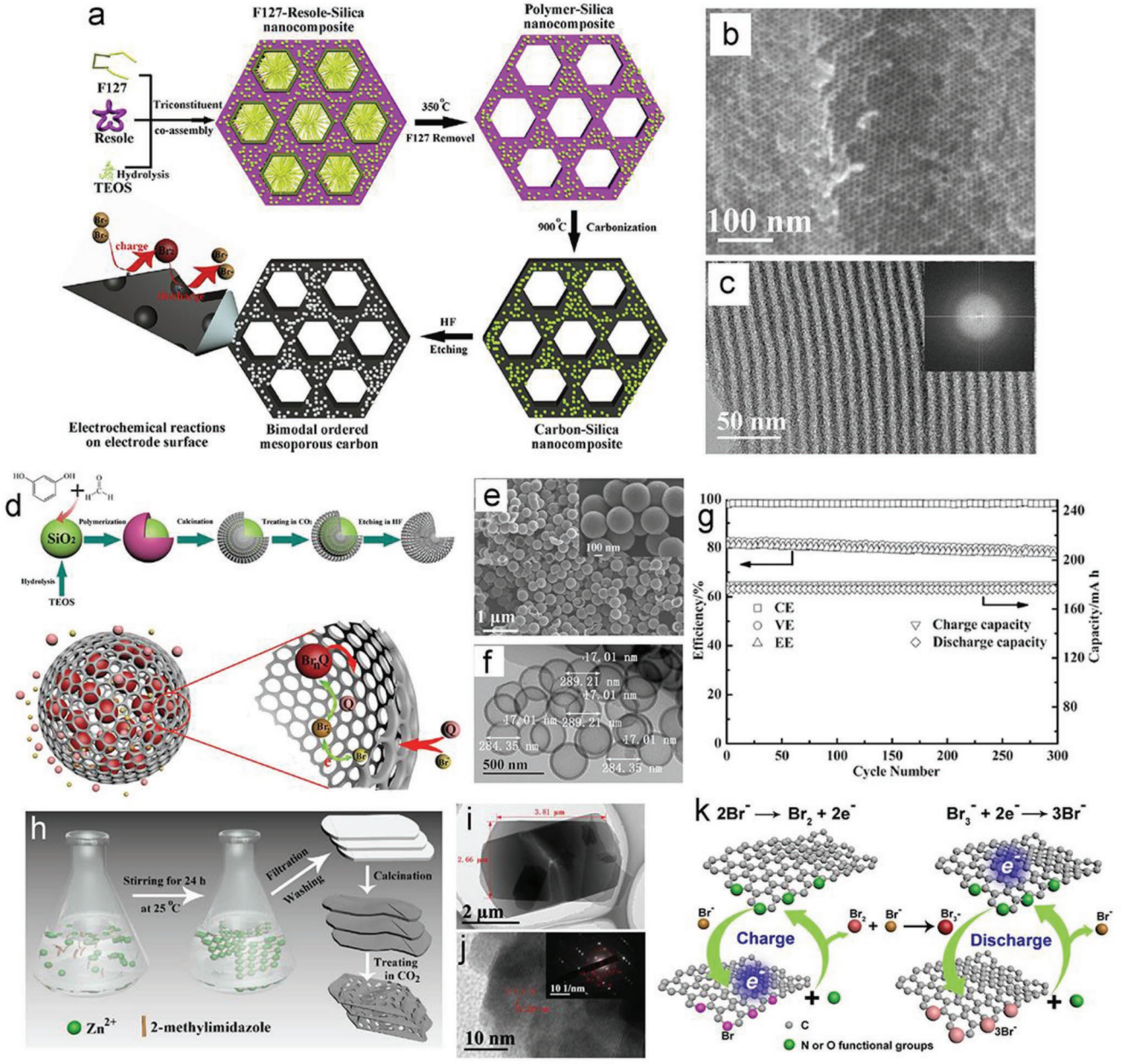

Figure 11. Carbon-based electrocatalyst for zinc–bromine flow battery. a) Synthesizing procedure of bimodal ordered mesostructure carbons (BOMCs). b) SEM image of BOMC-2. c) TEM image of BOMC-2. Reproduced with permission.[97] Copyright 2016, Elsevier Ltd. d) Schematic illustration to the fabrication and principle of cage-like porous carbon applied in zinc–bromine flow battery. e) SEM and f) TEM images of CPC. g) The performance of the zinc–bromine flow battery with CPC as electrocatalyst for bromine couple at the current density of 80 mA cm^{-2}. Reproduced with permission.[63] Copyright 2017, WILEY-VCH Verlag GmbH & Co. KGaA, Weinheim. h) Schematic illustration of the fabrication of porous nanosheet carbon. i) TEM and j) HRTEM of nanosheet zeolite-type metal organic framework (NSZIF). k) Catalytic mechanism of porous nanosheet carbon (PNSC) to bromine redox reaction. Reproduced with permission.[139] Copyright 2017, Elsevier Ltd.

and co-workers designed and fabricated a bimodal highly ordered mesostructured carbon (BOMC) electrode material through an evaporation-induced triconstituent co-assembly method that shows excellent electrocatalytic activity toward the bromine couple (**Figure 11**a).[97] By introducing a triblock copolymer (F127) and SiO_2 nanoparticles as dual templates and adjusting their ratio, the morphology (Figure 11b,c) of BOMCs can be well tuned, e.g., the hydrogen bond between resole and F127 induce ≈5 nm pores, and the removal of silica results in ≈2 nm pores on the 5 nm pore walls. These 2 nm pores on the 5 nm pore walls favor bromine adsorption and offer more active sites for the bromine couple, thus, providing an excellent electrocatalytic activity. As a result, a zinc–bromine flow battery with optimized BOMC as the positive electrode demonstrated a VE of 82.9% and an EE of 80.1% at a current density of 80 mA cm^{-2}, which is the best performance at such a high current density to be reported at that time.

© 2019 WILEY-VCH Verlag GmbH & Co. KGaA, Weinheim

Although BOMC demonstrates an excellent electrocatalytic activity toward the bromine couple and affords the zinc–bromine flow battery with an improved VE, the issue of bromine diffusion, which will result in serious self-discharge and an irreversible capacity decay, still remains. To simultaneously suppress the bromine diffusion and endow the bromine couple with improved activity, a cage-like porous carbon (CPC) with a specific pore structure was designed for the zinc–bromine flow battery.[63] By using SiO_2 as the template, formaldehyde and resorcinol were first polymerized via a hydrothermal reaction and then carbonized, with the carbon being activated by CO_2 to form pores on the shell. Finally, the CPCs were obtained by removing the SiO_2 template (Figure 11d). Similar to BOMC, the CPCs also demonstrate a superior activity toward the bromine couple on account of the abundant active sites generated during the CO_2 activation process. However, the most significant aspect of the work is that a pore size exclusion mechanism is applied in electrode material to suppress Br_2 diffusion. By varying the time of the CO_2 activation process, the morphology of CPCs (Figure 11e,f) can be well controlled, along with a pore size of ≈1.1 nm, which is just in between the size of Br^- (4.83 Å), MEP^+ (9.25 Å), and $MEPBr_3$ (12.40 Å). The pore size of CPCs can allow the free entrance of Br^- and MEP^+ into the cages. As long as the Br^- in the cages becomes oxidized to Br_2, the Br_2 will complex with MEP to form $MEPBr_3$ during the charging process. The $MEPBr_3$, with a larger size (12.40 Å), is then entrapped in the cavity with the small pore size (1.1 nm), thus, suppressing the bromine diffusion and further addressing the battery issue of self-discharge effectively. Combining the high Br_2-entrapping capability with an ultrahigh activity, the zinc–bromine flow battery with CPCs as the positive electrode material demonstrates a CE of 98% and an EE of 81% at 80 mA cm^{-2}, maintaining this performance for more than 300 cycles without evident decay (Figure 11g).

To further investigate the effects of the morphology, structure and surface properties of electrode materials on the electrocatalytic activity toward the bromine couple, a porous nanosheet carbon (PNSC) with a high activity was prepared for the zinc–bromine flow battery (Figure 11h) and investigated.[139] PNSC with in-plane pores (Figure 11i,j) was prepared by pyrolyzing a nanosheet zeolite-type metal organic framework (NSZIF) in carbon dioxide, which was obtained through a precipitation reaction between Zn^{2+} and 2-methylimidazole. During the pyrolyzing process, an abundance of N and O atoms from 2-methylimidazole can be doped into the PNSC. These heteroatoms possess higher electronegativities than that of the C atom, which makes the Br^- and Br_3^- anion species absorb on the carbon edge more easily and further form the adsorbent Br atom or Br^- through an electron transfer reaction (Figure 11k). Additionally, the N and O atoms in the PNSC can increase the electrode's hydrophilicity and further improve the wettability between the electrolyte and electrode. Moreover, this kind of material with a nanosheet morphology features a large specific surface area (2085.69 m^2 g^{-1}), short ion transfer pathway and high electronic conductivity, which result in a high activity and fast mass transport. In view of the aforementioned advantages, the PNSC can effectively boost the reaction rate of the bromine couple and further improve the performance of the zinc–bromine flow battery significantly.

As the bromine couple shows a poor kinetic reversibility and electrochemical activity on graphite felt (GF) electrodes, the case is the same with the iodine couple, which result in a low working current density and EE for the zinc–iodine flow battery.[111] To overcome this problem, introducing an electrocatalyst on GF surfaces seems to be an effective way. Metal–organic frameworks (MOFs) have always been treated as promising candidates on account of their extraordinarily high surface area and abundant pore geometries. Two MOFs, MIL-125-NH_2 and UiO-66-CH_3, have thus been adopted as effective electrocatalysts to facilitate the redox reaction of the iodine couple.[111] Different from the electrocatalysts used in the zinc–bromine flow battery, where the CCMs were adopted, the MOF electrocatalysts were dispersed on the GF surface through an in situ growth method. The cyclic voltammetry results reveal that these two MOFs exhibit an improved electrochemical activity and reversibility toward the iodine couple compared to those of the graphite material. Although MIL-125-NH_2 shows a better catalytic effect toward the redox reaction of the iodine couple than does UiO-66-CH_3, the chemical stability of MIL-125-NH_2 is lower than that of UiO-66-CH_3 in the zinc–iodine flow battery media, as proven by the cycling performance of the zinc–iodine flow battery. Because of the improved activity, the zinc–iodine flow battery with UiO-66-CH_3-modified GF as the positive electrode delivers a higher EE than that with pristine GF at 30 mA cm^{-2}, however, raising the EE value by 2.7%. The working current density is significantly enhanced compared with the author's previous work (10 mA cm^{-2}) because of the introduction of an electrocatalyst on the GF,[104] however, the stability of the MOFs in flow battery media as well as the battery performance still need to be further improved. In addition, the distribution of the MOFs on the GF surface should also be taken into further consideration.

Zinc metal is well known for its activity in chemistry, and thus, will undergo the hydrogen evolution reaction easily in acid media. This makes the zinc couple barely suitable for flow batteries that employ acid as the supporting electrolyte. The zinc–cerium flow battery has emerged as one of the few members that can be applied in acid media.[100,141–145] By using Ce^{3+}/Ce^{4+} as the positive couple, the zinc–cerium flow battery can afford a cell voltage ranging from 2.0 to 2.5 V in methanesulfonic acid media, which is the highest value among the proposed aqueous flow batteries. As such, the high potential of the battery together with the acidic electrolyte have brought forward a strong request for electrode materials, especially for positive electrode materials. Currently, the noble-metal-based materials are the most widely studied positive electrodes for the zinc–cerium flow battery.[146–151] However, the cost of these materials is relatively high, which has limited further application of the zinc–cerium flow battery. Thus, to develop novel electrode materials with a low cost and high performance that can displace costly noble-metal-based electrodes, Xie and coworkers investigated a homemade hierarchical porous carbon as an efficient positive electrode for the zinc–cerium flow battery.[152] This hierarchical porous carbon (HPC) was fabricated through a dual-templating method, of which a hard template and a soft template were employed, endowing the material with well-defined macroporous and mesoporous structures (**Figure 12**a,b). In this construction, the macroporous structure with pore sizes of 2 μm and 80 nm is obtained using the $Ni(OH)_2$ hard-template method. Meanwhile, the macroporous structure with a pore size of 10 nm is obtained using the

© 2019 WILEY-VCH Verlag GmbH & Co. KGaA, Weinheim

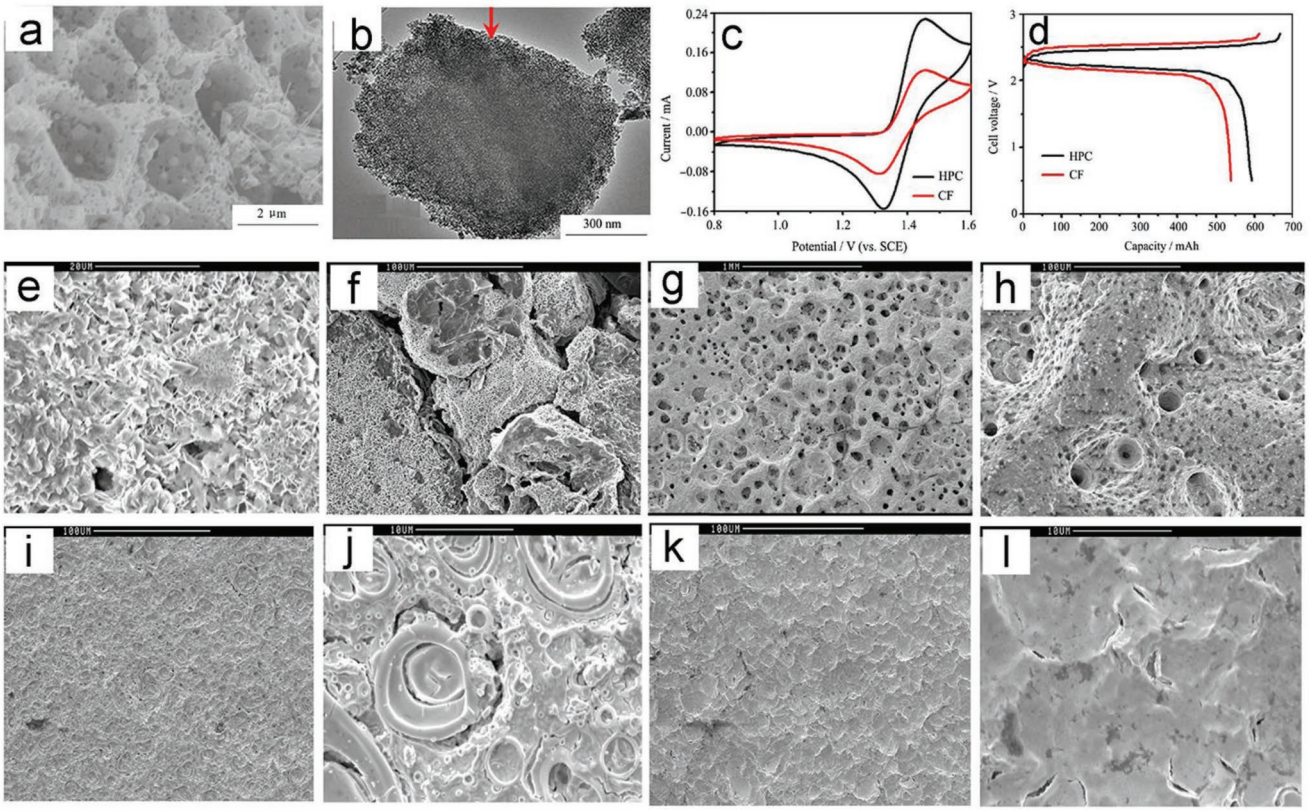

Figure 12. Electrodes for acidic zinc–cerium flow battery. a) SEM image and b) TEM image of hierarchical porous carbon (HPC). c) Cyclic voltammograms of Ce^{3+}/Ce^{4+} couple on HPC and carbon felt electrode (CF). d) The charge–discharge curves of the zinc–cerium flow battery with different positive electrodes. Reproduced with permission.[152] Copyright 2014, The Chinese Society of Rare Earths. Published by Elsevier B.V. Morphology of zinc deposited on e) HDPE-1 (high density polyethylene) and f) PVE (epoxies and vinyl esters) composite electrodes at 50 mA cm^{-2} for 2 min charging. Morphology of zinc deposited on g) HDPE-1 and h) PVE composite electrodes at 50 mA cm^{-2} for 5 min charging. Reproduced with permission.[153] Copyright 2013, Elsevier Ltd. Top-view SEM images of the surface of i,j) BMM3 (Pt/Ir50/50) electrode, k,l) SL2 (3 g Pt m^{-2}) electrode. Reproduced with permission.[154] Copyright 2014, Elsevier Ltd.

soft-template synthesis method, in which the self-assembly of organic templates via the reaction between phloroglucinol and polyethyleneoxide-*b*-polypropyleneoxide-*b*-polyethyleneoxide takes place. The macropores in HPC allow the diffusion of ions within the electrode, which can improve the polarization of the battery, while the mesopores are beneficial to increase the surface area of the electrode, thus, endowing the cerium couple with improved kinetics. This hierarchical pore structure in turn affords the HPC electrode with a better performance over that of the carbon felt electrode as displayed in Figure 12c,d. Nevertheless, the zinc–cerium flow battery with the HPC as the positive electrode only delivers an EE of 79.0% at 30 mA cm^{-2}, which is relatively low for practical applications. Therefore, novel electrode materials with a high performance remain urgently needed for the zinc–cerium flow battery.

Electrode for Negative Half-Cells: From the above description, we can see that tremendous efforts have been concentrated upon designing and modifying positive electrode materials to enhance the electrochemical performance of ZFBs, whereas little attention has been paid to the negative side, which results in a few relevant tactics for improving the batteries' areal capacity. In this regard, in-depth research on the behavior of zinc deposition at the negative electrode should be carried out, as it will be highly beneficial to boost the areal capacity of zinc-based flow batteries. For example, Zhao and co-workers recently conducted extensive research on the electrochemical behavior of zinc at a carbon electrode through theoretical and fundamental studies.[106] The first-principles study was conducted to investigate the zinc adsorption and diffusion on representative carbon surfaces, which include a pristine graphite (001) surface, two surfaces with vacancies (single vacancy and double vacancies), and three surfaces with oxygen-functional groups (epoxy group, carbonyl group, and hydroxyl group). The simulation results indicate that only single vacancies have an adsorption energy amenable toward zinc atoms, which results from its dangling carbon atoms with unpaired electrons. The dangling carbon atoms with unpaired electrons present a strong attraction to the electrons around zinc and thus improve the electron transfer. By contrast, the rest of the defective carbons (surfaces with double vacancies and three surfaces with oxygen-functional groups) present no improved adsorption abilities toward the zinc atom over that of the pristine surface, which is attributed to the fully occupied d- and s-orbitals of the zinc atom, making these electrons difficult to lose. As a result of the higher adsorption energy, the zinc atom is more inclined to deposit at a single vacancy site than on the pristine carbon surface. Additionally,

© 2019 WILEY-VCH Verlag GmbH & Co. KGaA, Weinheim

the deposited zinc atom tends to be anchored and becomes a nucleation site further zinc deposition, which results from the high diffusion barrier to transport away from the single vacancy. Thus, the zinc morphology and distribution can be well-tuned through varying the distribution of single vacancies on the negative electrode, which is expected to yield a uniform distribution of zinc during the plating of the battery. According to the above-mentioned theory, a thermally treated graphite felt negative electrode with abundant carbon defects was thus prepared and tested in a zinc–bromine flow battery. The results clearly indicate that the morphology of zinc deposited on the electrode with abundant carbon defects is considerably more uniform than that on the original graphite electrode with few defects; these observations provide new insights and novel methods to control the zinc morphology deposited on the negative electrode.

Except for the investigation of electrodes in neutral zinc-based flow batteries, the electrochemical behaviors of both positive and negative electrodes in the acidic zinc–cerium flow battery have also attracted wide-ranging attention.[100] For instance, Nikiforidis et al. undertook plenty of work on different electrode materials for both the positive and negative redox reactions of the acidic zinc–cerium flow battery.[153,154] To present a deep insight into the behavior of zinc deposition in acidic media, the authors first conducted an investigation into zinc deposition at the edges of different carbon materials. As previously mentioned, zinc dendrite is a common problem associated with zinc-based flow batteries. Normally, the growth of zinc dendrites indicates the heterogeneous distribution of potential and current on the surface of an electrode, resulting in a deposition that can be dislodged easily. Zinc dendrite is more likely to grow at the edge of an electrode rather than the center because of the higher overpotential at the electrode edge. Focusing at the edge of the electrode's surface, there are no signs of dendritic growth on a high-density polyethylene composite electrode (HDPE-1) (Figure 12e), whereas needle-shaped zinc can be found on the epoxy and vinyl ester (PVE) composite electrode (Figure 12f). However, a possible explanation for the different morphologies of zinc deposited on these electrodes has not been proposed. Further prolonging the charging time from 2 to 5 min affords a significant difference in the zinc morphology deposited on the same electrode (Figure 12g,h), where pinholes can be clearly observed. These pinholes are mainly derived from the adsorbed hydrogen and the subsequent hydrogen evolution reaction at these sites, both of which hinder the adhesion of the zinc to the surface. Hence, developing novel negative electrode materials that can effectively restrain the hydrogen evolution side reaction in acid media is still very important for the application of the zinc–cerium flow battery. In addition to negative electrodes, the authors then investigated the electrochemical behavior of the cerium couple on various Pt- and Pt–Ir-coated titania-based substrates.[154] Although only the surface morphologies of BMM3 (Pt/Ir50/50) (Figure 12i,j) and SL2 (3 g Pt m^{-2}) (Figure 12k,l) electrodes are provided, the characterization of the electrochemical properties of the cerium couple on the eleven electrodes is very comprehensive, and offers a reference for subsequent studies. However, the high cost of Pt-based electrodes will restrict their further application in the zinc–cerium flow battery, although they exhibit a relatively high stability in the electrolyte and reversibility for the cerium redox couple.

4.2.2. Electrode for Alkaline Zinc-Based Flow Batteries

As displayed in Figure 1, currently, alkaline zinc-based flow batteries mainly include the single zinc–nickel and air flow battery, zinc–iron flow battery, and zinc–iodine flow battery. Among which, the newly reported alkaline zinc–iodine flow battery is only at the starting stage.[105] As a consequence, there has yet to be any report of a new kind of electrode material for the alkaline zinc–iodine flow battery. However, the alkaline zinc–iron flow battery, although having been proposed very early on, has been rarely reported on, let along its electrode materials. Indeed, the kinetics and reversibility of the zinc and iron couples on the carbon felt electrode can satisfy the needs of practical applications,[59] promoting little research on electrode materials for the alkaline zinc–iron flow battery. Hence, the investigation on electrodes, and positive electrode materials in particular, has mainly focused on alkaline single zinc–nickel and air flow batteries since the kinetics of nickel hydroxide and oxygen electrodes is relatively sluggish,[155–160] which reduce the energy conversion efficiencies. The mismatch in kinetic activations between the positive and negative redox couples on the electrodes can result in zinc accumulation at the negative side, further affecting the battery's cycle life.[48]

Electrode for Positive Half-Cells: For the alkaline single zinc–nickel flow battery, the concentration of the alkaline supporting electrolyte is usually high (8 M or even higher). Under such conditions, with charging, the zinc often presents in the form of a spongy-like structure, which can easily fall off the electrode and further lower the battery's cycling stability. Furthermore, hydrogen evolution at the negative electrode with high current densities reduces the energy efficiency of the battery and causes zinc metal to peel off from the electrode as well. To address the above issues, Zhang and co-workers introduced 3D porous nickel foams (NFs) for the negative electrode in the single zinc–nickel flow battery,[161] featuring an open porous structure and high specific surface areas. The open pore structure of NFs favors reducing the internal resistance at the interface between the electrode and electrolyte and prevents zinc from detaching before the reaction. Meanwhile, the high specific surface area reduces the polarization of the electrode by lowering the realistic current density. Benefiting from the 3D porous structure, the zinc is almost deposited on the surface of the positive side (**Figure 13**a), whereas little zinc can be found on the opposite side of the NF (Figure 13b) when a single zinc–nickel flow battery using the NF as the negative electrode was charged at 20 mA cm^{-2} for 40 min; this behavior results from a reduced polarization of the negative electrode. As a consequence, a single zinc–nickel flow battery with a 3D NF as the negative electrode can afford a CE of 97.3% and an EE of 80.1% at 80 mA cm^{-2}, along with a significantly improved power density.

Electrode for Negative Half-Cells: Apart from the single zinc–nickel flow battery, a new alkaline single zinc–air flow battery system, which stems from the zinc–air battery, was proposed by Pan et al. in 2009.[102] The zinc–air battery was proposed by Sammells in 1982[162] and has attractive features including a high theoretical energy density of 1086 Wh kg^{-1} (including oxygen) and a very low cost,[71] showing promise in the application of powering portable devices and electric vehicles. However, challenges remain for the practical application of the zinc–air

© 2019 WILEY-VCH Verlag GmbH & Co. KGaA, Weinheim

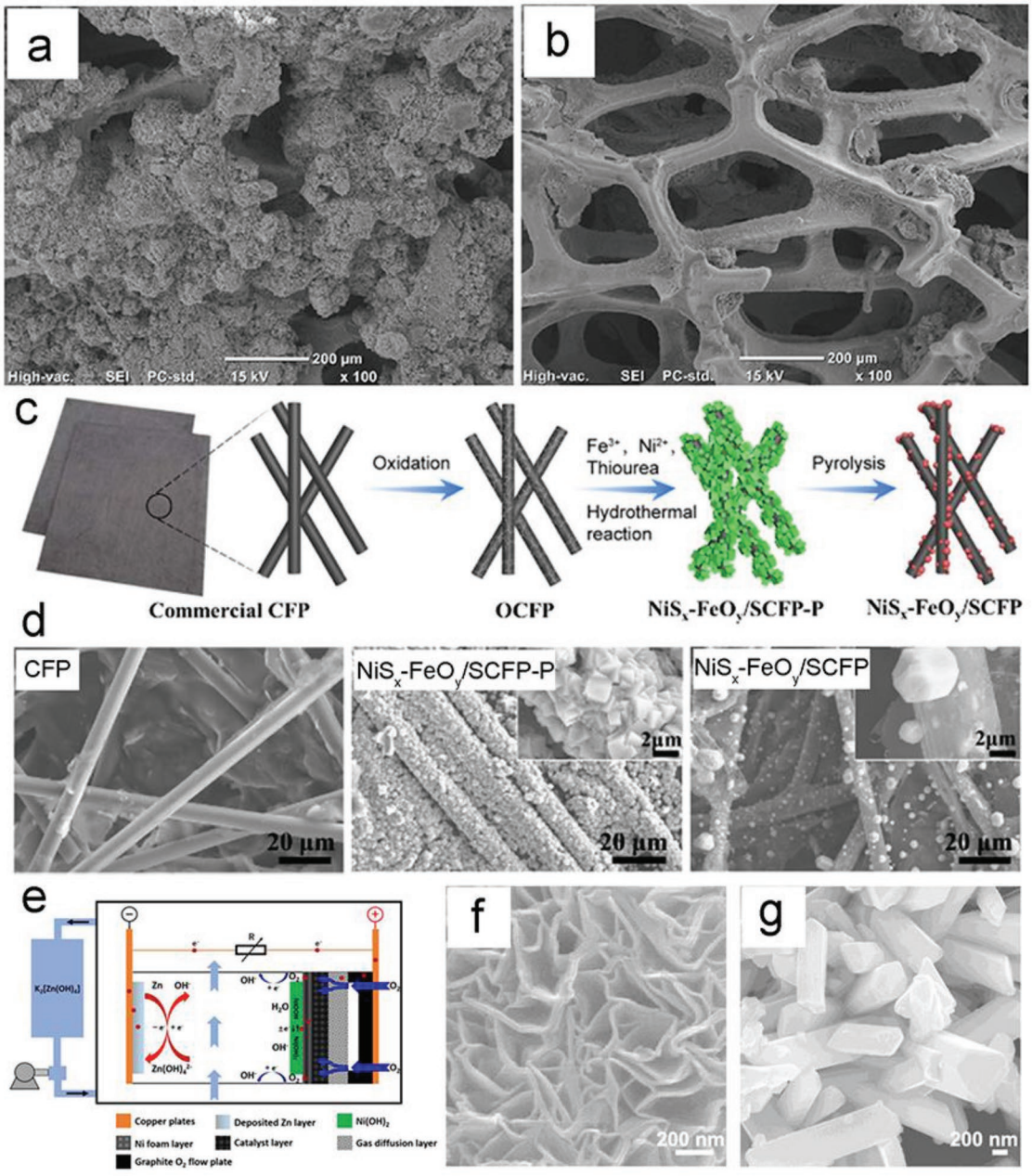

Figure 13. Electrodes for alkaline zinc–nickel or air flow battery. Morphology of zinc deposited on 3D porous nickel foams (NFs) at 20 mA cm^{-2} for 40 min a) near the positive electrode. b) Opposite side of NF. Reproduced with permission.[161] Copyright 2013, Elsevier B.V. c) The procedure for fabricating NiS_x–FeO_y/SCFP electrode for alkaline zinc–air flow battery. d) Morphologies of the corresponding materials. Reproduced with permission.[103] Copyright 2018, Elsevier Ltd. e) Illustration of the single flow Zn–$Ni(OH)_2/O_2$ hybrid battery. f) Morphology of $Ni(OH)_2$ and g) $Ag_4Bi_2O_5$ for a single flow Zn–$Ni(OH)_2/O_2$ hybrid battery. Reproduced under the terms of the Creative Commons Attribution License.[163] Copyright 2017, The Authors, Published by ESG.

battery, especially the zinc electrode and the air electrode. Considering the flowing electrolyte can reduce the thickness of the diffusion layer at an electrode and further minimize the concentration polarization of a battery, the issues accompanied by the zinc electrode, and its shape change caused by zinc dendrite in particular, can be effectively improved. As with the single zinc–nickel flow battery, the electrochemical reaction at the positive (air) electrode is limited since the kinetics of the oxygen reduction reaction (ORR) and the oxygen evolution reaction (OER), which take place at the triple phase boundary, are sluggish. This in turn results in a battery working at a low current density (normally under 20 mA cm^{-2}). Furthermore, the preparation of the air electrode, including the bifunctional air electrocatalysts employed to catalyze the OER and ORR, is complicated and tedious in comparison with that of the carbon felt electrode used in other flow battery technologies. Nevertheless, the design and preparation of OER and ORR catalysts for the electrically rechargeable single zinc–air flow battery is still

© 2019 WILEY-VCH Verlag GmbH & Co. KGaA, Weinheim

of the greatest importance. For instance, Xiang and co-workers recently designed an efficient unitary oxygen electrode for the alkaline single zinc–air flow battery by the in situ growth of amorphous NiS_x–FeO_y particles on sulfur-doped carbon fiber paper (referred to as NiS_x–FeO_y/SCFP, Figure 13c).[103] The in situ anchoring of amorphous NiS_x–FeO_y on sulfur-doped CFP (Figure 13d) endows the material with abundant accessible active sites and a very stable structure. Additionally, the synergetic effect of highly active NiS_x–FeO_y and 3D porous SCFP impart the NiS_x–FeO_y/SCFP with efficient pathways for reactants and electrons. Benefiting from these features, the NiS_x–FeO_y/SCFP can thus boost both the ORR and OER, affording a single zinc–air flow battery with a CE of 100% and a VE of 50% at a current density of 10 mA cm^{-2}, as well as a cycling stability of 110 h without performance decay.

Because the single zinc–air flow battery and single zinc–nickel flow battery have similar battery structures (membrane-free), Pan and co-workers creatively combined the single zinc–nickel flow battery with the single zinc–air flow battery and proposed a single flow zinc–nickel/air hybrid battery with a $Ni(OH)_2$–O_2 composite cathode in 2017 (Figure 13e).[163] However, such as the single zinc–nickel and air flow batteries, this hybrid battery also employs a high-concentration KOH-$K_2[Zn(OH)_4]$ as the electrolyte. The differences are that the anode is a copper foil with electrodeposited metallic zinc, and the cathode is a nickel hydroxide and oxygen composite electrode, where α-$Ni(OH)_2$ with nano/microcrystalline flakes (Figure 13f) and rod-shaped $Ag_4Bi_2O_5$ (Figure 13g) are employed as the active cathode material and the oxygen reduction catalyst, respectively. When the battery is charged, $Zn(OH)_4^{2-}$ is plated onto the negative electrode. In the meantime, $Ni(OH)_2$ is oxidized to NiOOH on the positive electrode, and no reaction takes place on the air electrode. The nano/microcrystalline flake structure of α-$Ni(OH)_2$ can enhance the diffusion of protons and electrons as well as the penetration of the electrolyte, further accelerating the electrochemical reaction of the electrode. While discharging, the reverse process occurs. The oxygen reduction reaction occurs at the end of the discharge process in the presence of the $Ag_4Bi_2O_5$ oxygen reduction catalyst, consuming the residual zinc metal in the negative electrode that comes from the zinc accumulation during the discharging process or the zinc plated on the copper foil. With such a device configuration, the hybrid battery can afford a CE of 99.2% and an EE of 84.2% at 20 mA cm^{-2}. Additionally, at the end of the discharge, no zinc dendrites are accumulated on the negative electrode. The novelty of this configuration is to be commended. However, further insight into this hybrid battery still raises questions since only an oxygen reduction catalyst is employed. This means that the ORR reaction will consume the zinc metal that electrodeposits on the copper foil when there is no zinc accumulation on the negative electrode, which leads to an electrochemical corrosion of the electrode. In addition, the high alkaline concentration of the electrolyte (8 M KOH and 20 M LiOH) may also result in severe zinc corrosion and further consumption of the zinc metal. As the cycling proceeds, the ORR reaction will stop working once the zinc metal deposited on the copper foil is completely consumed. Thus the bifunctional OER and ORR catalyst seems to be an effective solution to address this issue.

4.3. Electrolyte

The electrolytes, which are made up of active materials, supporting electrolytes and additives, serve as important media to store and release energy.[67,164] Thus, the properties of the electrolytes including the solubility,[165] conductivity,[166,167] and stability[168–170] have significant effects on the performance and cycling stability of ZFBs. The standards for the option of including a supporting electrolyte are based on the electrochemical kinetics of the active species at the electrode–electrolyte interface, the electrolyte solubility, and a minimal cross-contamination of the active materials.[67,171] A comprehensive overview of the electrolytes for zinc-based flow batteries requires a well-organized and meticulous design. However, we will mainly concentrate on the universal issues associated with the electrolytes used in zinc-based flow batteries, which include the concentrations of active materials in the supporting electrolytes, the stability of the active materials, the influence of additives on the battery performance, and the design of novel positive redox couples with high electrochemical kinetics and high solubility. Included with the above-proposed issues in the following section will be briefly summarized strategies, serving as a reference for the existing and future ZFB systems.

4.3.1. Electrolyte for Neutral or Acidic Zinc-Based Flow Batteries

The concentration of the active material is of very important for ZFBs' practical applications, as this determines the energy density of the battery.[23] The concentration of the active material is strongly dependent on the supporting electrolyte, additive and temperature.[172,173] Altering the existence forms of the active material is an efficient way to advance the concentration or to enhance the utilization of the active material. For instance, bromine and iodine normally exhibit a low solubility in aqueous media, which results in a high vapor pressure and corrosiveness. This behavior in turn significantly impacts the battery energy density and can be a source of safety issues.[116] Transforming bromine or iodine into a polybromide or polyiodide ion through a complexation reaction between the bromine and bromide ion (iodine and iodide ion) can evidently enhance the concentration of bromine (iodine). However, the use of the bromide ion as the complexing agent leads to a low utilization of the active material and further reducing the energy density of a battery. Thus, to liberate the bromide ion that is employed to capture the bromine and to further increase the utilization of the active material, a series of bromine organic salts (**Figure 14**a), such as *N*-ethyl-*N*-methyl pyrrolidinium bromide (MEP), 1-ethylpyridinium bromide ($[C_2Py]Br$) and 1-(carboxymethyl) pyridine-1-ium (QBr1), have been designed and proposed as novel bromine complexing agents (BCAs).[174,175] The utilization of these complexing agents can suppress the bromine crossover from positive to negative electrolyte because of the large size of the organic salts, thus, further increasing the CE of the battery. The complex agents developed early on, such as MEP, can allow elemental bromine to be isolated from an aqueous electrolyte in the form of a dense polybromine oil phase (heavy dense phase) that sinks to the bottom of the storage tank. During the discharge process, the dense polybromine oil phase is pumped into the battery, which

© 2019 WILEY-VCH Verlag GmbH & Co. KGaA, Weinheim

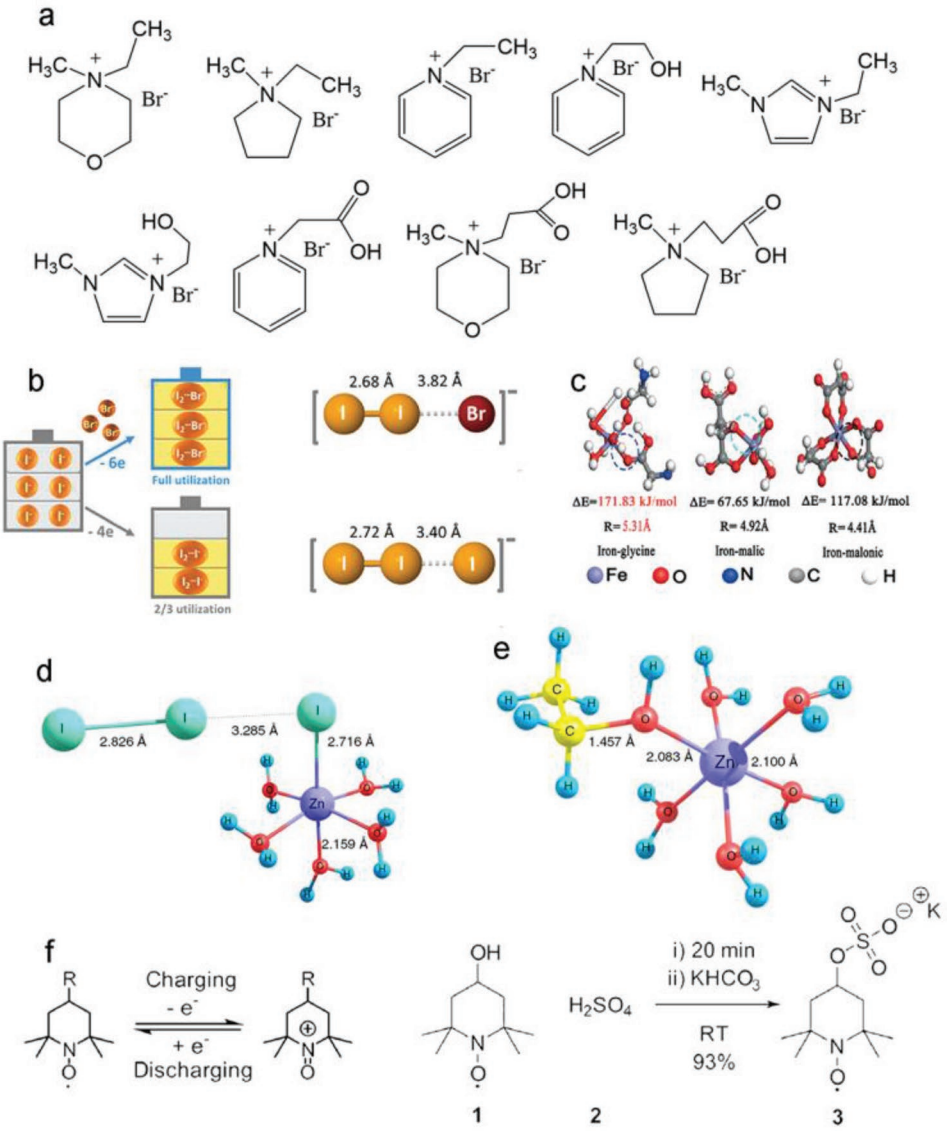

Figure 14. Electrolytes for neutral or acidic zinc-based flow batteries. a) Complexing agents for bromine couple. b) Concept illustration of bromide as the complexing agent to stabilize iodine. Reproduced with permission.[57] Copyright 2017, The Royal Society of Chemistry. c) DFT-optimized molecular structure of the anolyte in the neutral zinc–iron flow battery. Reproduced with permission.[61] Copyright 2017, Wiley-VCH Verlag GmbH & Co. KGaA, Weinheim. d) DFT-optimized molecular structure of the triiodide-complexed zinc cation. e) DFT-optimized molecular structure of the EtOH-complexed zinc cation formed in the catholyte during the charging process. Reproduced under the terms of the Creative Commons Attribution 4.0 International License.[104] Copyright 2015, Springer Nature. f) Synthesis of TEMPO derivative. Reproduced with permission.[62] Copyright 2017, American Chemical Society.

results in an inhomogeneous distribution of the positive electrolyte on the electrode and a further lowering of the battery performance. On the other hand, the partially dense polybromine oil phase may deposit on the electrode or at the interface between the electrode and current collector, which decreases the wettability between the electrolyte and the electrode (or the uniform contact of the interface between the electrode and current collector). This action further leads to a small part of the bromine participating in the electrochemical reaction, which in turn results in zinc accumulation at the negative side and further decreases the cycle life of the battery. The oil phase also requires a complicated network of pipes, pumps and automated controls to ensure access to the active material during discharge,[174] thereby increasing the system cost. To address the above issues, novel complexing agents containing carboxyl or hydroxyl group have been designed and proposed. These novel complexing agents not only effectively capture the electrogenerated bromine but also keep the bromine in the aqueous phase, which can undoubtedly improve the VE of the zinc–bromine flow battery. Nevertheless, the homogeneous electrolyte can also lead to bromine crossover and further result in the self-discharge of the battery. Thus, further studies of molecular design to synthesize novel complexing agents with both a high performance and large size should be carried out in the future.

Like the zinc–bromine flow battery, a similar complexing strategy has been applied in the zinc–iodine flow battery.[57] The

© 2019 WILEY-VCH Verlag GmbH & Co. KGaA, Weinheim

discharge energy density of the first reported zinc–iodine battery reaches as high as 167 Wh L^{-1} by using a 5 M ZnI_2 electrolyte.[104] This high energy density is due to the highly soluble iodide/triiodide (I^-/I_3^-) couple. However, to ensure the high reversibility of the iodide/triiodide (I^-/I_3^-) couple, only two-thirds of the iodide capacity is utilized, as one-third of the iodide ions have to serve as the complexing agent to stabilize iodine (I_2) by forming I_3^- (I_2I^-). To free one-third of the iodide ions and further increase the capacity of the zinc–iodine flow battery, Lu and co-workers tactfully exploited bromine ions,[57] which are substantially more abundant and cheaper than iodide, as the complexing agent to stabilize the iodine (I_2) and liberate one-third of the iodide ions that serve as the complexing agent to stabilize iodine (I_2) (Figure 14b). To avoid the formation of bromine during the charging process of the battery, the cut-off voltage of the zinc–iodine/bromine flow battery is strictly controlled and is lower than that of the zinc–bromine flow battery. Regardless, the energy density of the battery can still reach 202 Wh $L_{posolyte}^{-1}$ because of the increased capacity resulting from the liberated iodide ions. To further enhance the energy density of the flow battery, Chen and co-workers proposed an alkaline zinc–iodine flow battery in 2018,[105] of which the strategy for enhancing the potential of the battery by tuning the pH of the electrolyte is employed. The enhanced potential of the battery ultimately increases the energy density of the battery to 330.5 Wh L^{-1}, which is the highest value among all-aqueous flow batteries. Indeed, the discharge energy density and working current density of these zinc–iodine flow batteries can be further improved by developing new ion-conducting membranes with reduced impedance.

As the carrier of electric energy, the stability of the active material has a significant effect on the performance, energy density and cycle life of ZFBs.[168,169] To improve the energy density and cycle life of the zinc-based flow battery, guaranteeing the stability of the active materials in the supporting electrolytes is inevitable. Taking the Fe^{2+}/Fe^{3+} redox couple as an example, the species form a promising positive redox couple because of the high solubility, excellent kinetics and reversibility in acidic media,[68] however, this couple is not stable in neutral media because of the hydrolysis of iron ions. This reaction will in turn decrease the energy density and cycle life of the battery. For instance, Xie and coworkers put forward a strategy to stabilize the Fe^{2+}/Fe^{3+} redox couple by employing 1.5 M H_2SO_4 as the positive supporting electrolyte for a zinc–iron flow battery.[60] Although the high concentration of protons can prevent the Fe^{2+}/Fe^{3+} couple from hydrolyzing, the efficiency and cycling stability (an EE of 71.1% after 50 cycles at 30 mA cm^{-2}) of the battery still need to be further improved. Even though an Ac^-/HAc buffer solution was employed as the negative supporting electrolyte, the protons in the positive side can be easily transferred through the membrane to the negative side and react with the zinc metal during the charge process, further leading to the fading of the battery's capacity and the loss in CE.

To further improve the performance and cycle life of the zinc–iron flow battery, Li and co-workers innovatively conceived of an idea to stabilize the Fe^{2+}/Fe^{3+} couple and simultaneously prevent the crossover of the iron ions by introducing a complexing agent.[61] Through optimizing the architecture of complexing agents, glycine was determined to exhibit the best complexation ability among those of malic and malonic acid because of the strong bonding force between glycine and irons, which was proven by DFT calculations (Figure 14c). Meanwhile, the conductivity of the electrolyte can be assured using KCl as the supporting electrolyte, which can endow the battery with a VE of 88.65% at a current density of 40 mA cm^{-2}. Although the sagacious strategy results in the neutral zinc–iron flow battery becoming a very promising candidate for energy storage applications, the long-term stability of the battery requires further investigation.

Before implementing the studies into an active material's stability, it is of vital importance to gain insight into what forms of the active material are in supporting electrolyte. Additionally, the corresponding strategies to enhance the stability of the active material can thus be further presented. A case in point is the solution chemistry of the ZnI_2 electrolyte in a neutral zinc–polyiodide flow battery implemented by Wang and co-workers.[104] The authors first reported a high energy density neutral zinc–polyiodide flow battery for various energy storage applications and then thoroughly studied the stability (in terms of temperature and state of charge (SOC) range) of the liquid ZnI_2 electrolyte via both off-line static and on-line cycling tests. Both off-line and on-line cycling tests demonstrate that the electrolytes were stable at a high temperature (50 °C), whereas the stability of the fully charged catholyte at low temperature (0 °C) appears to be an issue. I_2 precipitation can easily occur at 0 °C for a battery with 2.5 and 3.5 M ZnI_2 electrolytes at 100% SOC after 10 days of storage, which results from the interactions between the zinc and iodide species. Nuclear magnetic resonance (^{67} Zn NMR) and density functional theory (DFT)-based simulations indicate that the low energy barrier (≈0.2 eV) for the triiodide dissociation in the zinc-complexed form (Figure 14d) can result in the formation of molecular iodine, which is known to possess a low solubility in aqueous solutions. Based on these results, controlling the complexing agent of the Zn^{2+} can be an efficient way to prevent the I_2 from sedimentation, and the approach is different from the strategies using complexing agents to stabilize the I_2. To realize this concept, ethanol (EtOH) was introduced into the electrolyte, which can on one hand improve the stability of the electrolytes at a low temperature (–20 °C) and on the other hand mitigate the issue of zinc dendrites. The improved electrolyte's stability is realized by replacing a water molecule from the primary solvation shell of Zn^{2+} with an EtOH (Figure 14e). The zinc dendrite mitigation is believed to result from the EtOH coordination with Zn^{2+}, which improves the plating overpotential and thereby reduces the plating exchange current density, further leading to a smooth zinc surface. The presented results provide a fundamental research approach to the investigation of an electrolyte's stability.

Recently, some new ZFBs coupled with organic redox-active compounds were designed and reported by Schubert and co-workers;[62] the TEMPO-containing polymer, P(TEMPO-*co*-PEGMA (poly(ethylene glycol)methyl ether methacrylate))s and P(TEMPO-*co*-METAC ([2-(methacryloyloxy)ethyl]trimethylammonium chloride))s were thus designed as cathode active materials,[22,114] which broadened the species available for ZFBs. However, the solubility of these materials is very limited, which will result in a battery with a low energy density. To enhance the solubility, the authors straightforwardly synthesized a sulfate-potassium-salt-containing TEMPO derivative through molecular design (Figure 14f). An elevated concentration of

© 2019 WILEY-VCH Verlag GmbH & Co. KGaA, Weinheim

1 M cathode active material in an NH_4Cl supporting electrolyte can be afforded because of the introduction of the sulfate potassium salt. Benefiting from the improved solubility of the cathode active material, the capacity of the catholyte can be raised dramatically from 2.4 to 26.7 Ah L^{-1}, compared to that of the previously reported zinc–poly TEMPO flow batteries, thus, further endowing the battery with an improved energy density of 20.4 Wh L^{-1}. Nevertheless, the concentration of the cathode active material (35×10^{-3} M) and the working current density (3 mA cm^{-2}) of this battery still need to be improved.

4.3.2. Electrolyte for Alkaline Zinc-Based Flow Batteries

As previously mentioned, the current investigations on alkaline zinc-based flow batteries are mainly concentrated on alkaline single zinc–nickel and air flow batteries.[47,48,102,110,176,177] The components of the electrolytes for alkaline single zinc–nickel and air flow batteries are relatively straightforward and are mainly comprised of the zincate active material and alkaline supporting electrolyte. As a consequence, relatively few studies on the electrolytes used in alkaline zinc-based flow batteries have been reported, and of those that have been reported, the organic or inorganic electrolyte additive is mostly studied for the sake of inhibiting the growth of spongy zinc during the charging process. The spongy zinc metal can be easily formed from an alkaline zincate solution and can easily detach from the substrate and further affect the cycle stability of the battery.[178–181] To address this issue, Wen and coworkers performed several studies on the effects of inorganic and organic additives on suppressing spongy zinc electrogrowth.[182,183] For alkaline zinc-based flow batteries, inorganic additives must meet the following requirements: 1) they must be soluble in alkaline media, and 2) their standard potentials should be higher than that of the zinc. For example, soluble PbO and Na_2WO_4 were selected as additives to investigate their influence on the electrochemical behavior of zinc, of which the surface morphology of the zinc deposits on the nickel electrode after 210 min charging at 20 mA cm^{-2} was examined (the zinc–air electrolysis cell was employed as the platform). Without additives in the electrolyte, spongy zinc with a 3D structure can be clearly found (**Figure 15**a,d), whereas the formation of spongy zinc is effectively restrained by the addition of 5×10^{-5} M PbO (Figure 15b) or 0.6 M Na_2WO_4 (Figure 15e). The morphology change in the zinc is mainly attributed to the increased polarization of the electrode, which results from the addition of additives to the electrolytes. The increased polarization of the electrode

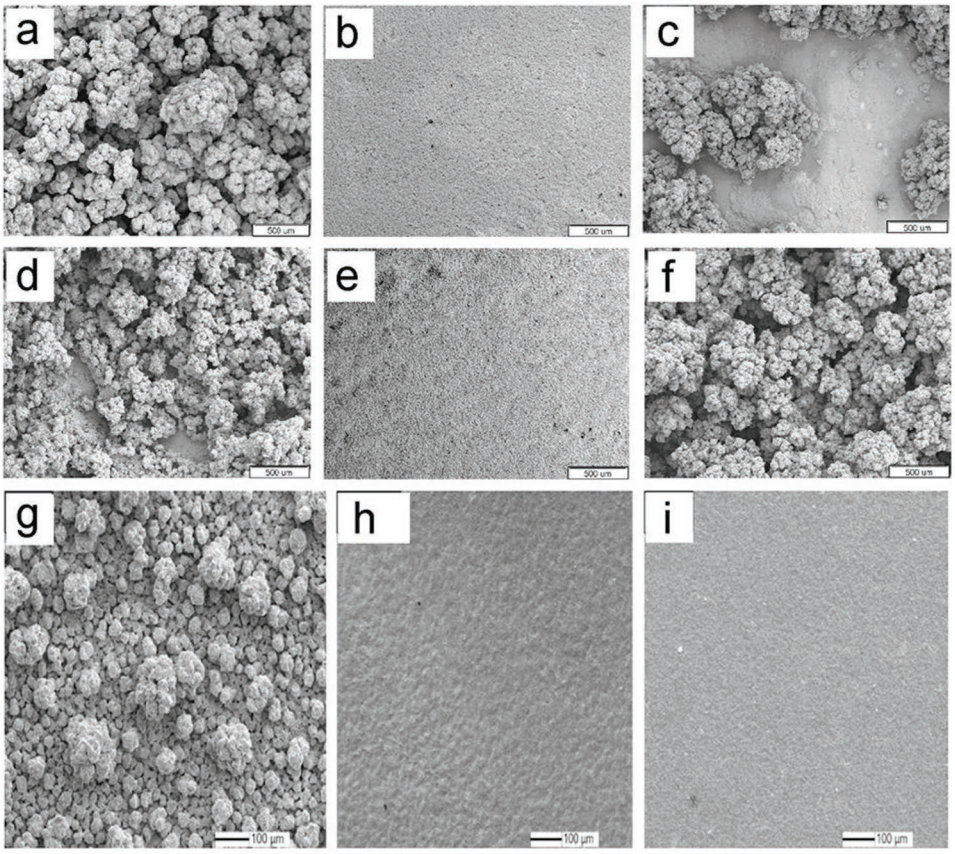

Figure 15. Effects of additives on zinc morphology in the alkaline zinc-based flow batteries. Morphology of zinc deposits in the presence of lead ions with different concentrations a) 0 M. b) 5×10^{-5} M. c) 10^{-3} M. Morphology of zinc deposits in the presence of tungstate ions with different concentrations d) 0.4 M. e) 0.6 M. f) 1.0 M. Reproduced with permission.[183] Copyright 2009, Elsevier B.V. Morphology of zinc deposits in the presence of g) alkaline blank solution h) 10^{-4} M Pb^{2+} and i) 10^{-4} M $Pb^{2+} + 5 \times 10^{-5}$ M tetrabutylammonium bromide (TBAB). Reproduced with permission.[182] Copyright 2011, Elsevier Ltd.

© 2019 WILEY-VCH Verlag GmbH & Co. KGaA, Weinheim

in turn slows the rate of zinc deposition during charging and thereby changes the zinc morphology. Nevertheless, the further increase in the polarization decreases the cell performance. Further increasing the concentration of the additives yields a mixed spongy and compact zinc morphology for the electrolyte with PbO as the additive (Figure 15c), while a complete spongy zinc can be found for the electrolyte with Na_2WO_4 as the additive (Figure 15f). The scientific reason behind this phenomenon has yet to be further clarified.

To verify the practicability of the additives in alkaline zinc-based flow batteries, the influences of organic additives on the zinc morphology were also studied in the alkaline single zinc–nickel flow battery. A similar spongy and granular zinc morphology can be observed (Figure 15g) on a polished nickel sheet substrate after electro-deposition at the cathodic overpotential (η = –100 mV) when using an additive-free solution. It has been claimed that the addition of 10^{-4} M Pb^{2+} affords a less open and relatively compact zinc morphology together with some pits and hollow features (Figure 15h), whereas the addition of 10^{-4} M Pb^{2+} + 5×10^{-5} M tetrabutylammonium bromide (TBAB) produces a dense, smooth and compact zinc morphology (Figure 15i), indicating the excellent inhibition ability of the additives toward the spongy zinc growth. The authors attributed this dense, smooth and compact zinc morphology to the synergistic effect of Pb^{2+} and TBAB on the inhibition of spongy zinc. However, the morphology of zinc using TBAB as the individual additive was not provided, although the effects of the TBAB concentration on the current–time profile were given. Additionally, the mechanisms behind inhibiting the spongy zinc growth using different types of additives should be further clarified. The addition of additives to the electrolytes appears to be an effective way to inhibit the formation of spongy zinc in alkaline media and may be used in other alkaline zinc-based flow battery systems, e.g., the alkaline zinc–iron flow battery and the alkaline zinc–iodine flow battery. Additionally, a systematic in-depth study on the morphology of zinc deposited on a 3D porous electrode, such as carbon felts, in the presence of additives in the electrolytes should be further carried out since not every kind of alkaline zinc-based flow battery adopts a plate substrate for the electrodes. The influences of the additives in the electrolytes on the electrochemical performance, including the cycling stability of the batteries, should also be assessed, and the relationship between the zinc morphology and the electrochemical performance of the batteries can thus be correlated to provide technical support for practical applications of alkaline zinc-based flow batteries.

As previously mentioned, currently the categories of alkaline zinc-based flow batteries are very limited, e.g., single zinc–nickel and air flow battery and zinc–iron flow battery due to the fact that the categories of positive redox couples in alkaline media are very limited. Taking the advantage of the large negative redox potential of $Zn/Zn(OH)_4^{2-}$ in alkaline media (–1.22 V vs SHE), quite recently, Aziz et. al. reported a high voltage aqueous zinc–organic hybrid flow battery by utilizing a three-electrolyte, two-membrane configuration,[184] which is similar to the previous amphoteric zinc–iron flow battery and zinc–cerium flow battery.[56,185] By pairing an alkaline negative electrolyte comprising a $Zn/Zn(OH)_4^{2-}$ redox couple with an acidic positive electrolyte comprising high potential organic frog quinone molecule (FQ) redox couple, the proposed flow battery can operate at a high operating voltage of 2.0 V. Although a two-membrane (Nafion 117 and Selemion DSV) was employed for the battery, the OH^- and H^+ in negative and positive electrolytes will migrate to the middle neutral electrolyte, and finally an acid-base reaction will occur irreversibly. This irreversible acid–base reaction will result in a decreased concentration of acid and alkaline in the electrolytes and further reducing the battery performance.

5. Conclusions and Outlooks

ZFBs have proven to be one of the most promising solutions for stationary energy storage. Although remarkable performances have been achieved for ZFBs through extensive research on advanced materials, challenges still need to be overcome to realize the commercialization and industrialization of these devices. The power density, the cycle life and even the energy density need to be further improved. To realize the industrialization of ZFBs, advanced materials with a low cost remain in urgent need.

5.1. Designing and Fabricating High Performance Membrane Materials

Perfluorinated cation exchange membranes are currently the most widely used membranes in ZFB systems. However, these membranes are mostly suitable for acidic battery systems, since the protons are more favored to pass through these membranes. Unfortunately, ZFB systems are normally in neutral and alkaline media, as zinc metal is not stable in acid solutions. Other membranes encounter numerous problems in different ZFB systems, e.g., anion exchange membranes experience degradation in alkaline media, most aromatic-based membranes cannot withstand the highly oxidizing bromine, and dense membranes normally exhibit a relatively high area resistance in neutral media. Porous membranes have been regarded as one of the best choices for ZFBs, since they have been proven feasible in many ZFB systems. Therefore, aiming at the differences among several ZFB systems; designing and manufacturing porous membranes with a high performance from the perspective of materials and structure; and optimizing the membrane morphology by means of blending, coating, layer-by-layer technologies, etc. to endow the membranes with various functionalities have served as development directions. Nevertheless, innovative polymer materials through molecular design that can endow membranes (porous or dense) with a high performance should also be taken into account.

5.2. High Performance Electrode Materials with Enhanced Areal Capacity

Carbon-based materials such as carbon felt, carbon cloth, and carbon paper are the most widely used positive electrodes for most ZFB systems on account of their high activity and reversibility toward positive redox couples. However, the operating current density of ZFBs is still quite low. Thus, developing electrode materials with a high performance remains necessary, especially for those redox couples with low kinetics, e.g.,

© 2019 WILEY-VCH Verlag GmbH & Co. KGaA, Weinheim

the bromine (iodine) redox couple, cerium redox couple and TEMPO-based redox couple. Furthermore, additional investigations on positive electrodes for the alkaline single zinc–nickel and air flow batteries should be carried out to accelerate the progress of these batteries, aiming to increase the capacity of the nickel electrode and enhance the kinetics of the ORR and OER at the air electrode. Currently, the negative electrodes for ZFBs can be classified into two categories according to their structure: plate electrodes and porous electrodes. The plate electrodes, which are extensively applied in alkaline single zinc–nickel and air flow batteries because of their plug-in cell configuration, normally result in the battery working at a relatively low current density as a result of the limited active sites, further providing the battery with a low power density. Therefore, porous electrodes, and porous carbon electrodes in particular, serve as the main negative electrodes for zinc-based flow batteries at present. As one of the common problems associated with ZFBs, the volume or space of negative electrodes tend to lead to batteries with a limited capacity. Thus, how to employ this available volume or space to obtain a more uniformly dense zinc layer on the electrode is very important to increasing the batteries' capacities. Moreover, the electrochemical behaviors of deposition on different electrode materials in different electrolyte media (especially in alkaline media) need to be further clarified to provide technical support for achieving a uniformly dense zinc layer. Additionally, the combination of membranes, electrodes and electrolytes together for the effective prevention of zinc dendrites is necessary to afford ZFBs with a long cycle life.

5.3. High Concentration Electrolytes with High Stability

Designing novel redox couples and further novel flow battery systems has always been a research hotspot in the area of flow batteries. These fundamental studies are necessary to push forward the progress of flow battery technology. Thus, a wide variety of ZFB technologies have been proposed, and various electrolytes have been derived. Nevertheless, the current issues associated with the electrolytes do not focus on insufficient species of the positive redox couples but revolve around the stability, solubility and ion conductivity of electrolytes. Compared with investigations into the membranes and electrodes, investigations into electrolytes, with the exception of redox couples, are relatively fewer, especially those dealing with the chemistries of the redox couples in their corresponding supporting electrolytes, and this has resulted in a few relevant strategies for addressing the above issues. Thus, further research should be focused on the scientific understandings of the fundamental aspects of the electrolytes. In addition, the effects of the supporting electrolytes and additives on the electrochemical behavior of the zinc plating/stripping process should also be further explored to afford a dendrite-free ZFB with a long cycle life. To accelerate the forward progress of ZFB technologies, building a compendium of the well-understood electrolytes, membranes and electrodes within a defined battery system is also very important.

This review summarizes the strategies for modifying advanced materials to overcome the limitations of ZFB technologies, together with discovery of novel battery chemistries. We believe that with the progress of advanced materials, ZFB technologies have great potential to engage in practical applications for stationary energy storage applications.

Acknowledgements

The authors greatly acknowledge the financial support from Dalian science and technology innovation project (2018J12GX050), CAS STS program, NSFC (U1808209), Key project of Frontier Science, CAS (QYZDB-SSW-JSC032), DICP funding (DICP ZZBS201814 and ZZBS201707), Youth Innovation Promotion Association CAS, Major Scientific and Technological Innovation Project of Shandong (2018YFJH0106), and the Key Project of Natural Science Foundation of Liaoning Province (Grant No. 20180540128).

Conflict of Interest

The authors declare no conflict of interest.

Keywords

advanced materials, electrochemistry, energy storage, zinc dendrite and accumulation, zinc-based flow battery

Received: March 30, 2019
Revised: June 22, 2019
Published online:

[1] S. Chu, Y. Cui, N. Liu, *Nat. Mater.* **2017**, *16*, 16.
[2] B. Obama, *Science* **2017**, *355*, 126.
[3] BP Energy Outlook 2018 edition, **2018**.
[4] B. R. Chalamala, T. Soundappan, G. R. Fisher, M. R. Anstey, V. V. Viswanathan, M. L. Perry, *Proc. IEEE* **2014**, *102*, 976.
[5] H. Ibrahim, A. Ilinca, J. Perron, *Renewable Sustainable Energy Rev.* **2008**, *12*, 1221.
[6] P. F. Ribeiro, B. K. Johnson, M. L. Crow, A. Arsoy, *Proc. IEEE* **2001**, *89*, 1744.
[7] T. N. Cong, *Prog. Nat. Sci.* **2009**, *19*, 1297.
[8] Z. Yuan, H. Zhang, X. Li, *Chem. Commun.* **2018**, *54*, 7570.
[9] C. Zhang, L. Zhang, Y. Ding, S. Peng, X. Guo, Y. Zhao, G. He, G. Yu, *Energy Storage Mater.* **2018**, *15*, 324.
[10] G. L. Soloveichik, *Chem. Rev.* **2015**, *115*, 11533.
[11] B. Schwenzer, J. Zhang, S. Kim, L. Li, J. Liu, Z. Yang, *ChemSusChem* **2011**, *4*, 1388.
[12] C. Ponce de León, A. Frías-Ferrer, J. González-García, D. A. Szánto, F. C. Walsh, *J. Power Sources* **2006**, *160*, 716.
[13] L. Li, S. Kim, W. Wang, M. Vijayakumar, Z. Nie, B. Chen, J. Zhang, G. Xia, J. Hu, G. Graff, J. Liu, Z. Yang, *Adv. Energy Mater.* **2011**, *1*, 394.
[14] X. Li, H. Zhang, Q. Zheng, J. Yan, Y. Guo, Y. Hu, *Bull. Chin. Acad. Sci.* **2019**, *34*, 443.
[15] W. J. Lu, Z. Z. Yuan, Y. Y. Zhao, H. Z. Zhang, H. M. Zhang, X. F. Li, *Chem. Soc. Rev.* **2017**, *46*, 2199.
[16] H. Zhang, *Nature* **2014**, *508*, 319.
[17] W. Lu, C. Xie, H. Zhang, X. Li, *ChemSusChem* **2018**, *11*, 3996.
[18] F. R. M. a. E. J. Cairns, *J. Electrochem. Soc.* **1991**, *138*, 645.
[19] G. Adams, R. Hollandsworth, B. Webber, *Rechargeable Alkaline Zinc/Ferricyanide Battery*, Report 1, Lockheed Missiles and Space Co., **1979**.
[20] A. Khor, P. Leung, M. R. Mohamed, C. Flox, Q. Xu, L. An, R. G. A. Wills, J. R. Morante, A. A. Shah, *Mater. Today Energy* **2018**, *8*, 80.

 © 2019 WILEY-VCH Verlag GmbH & Co. KGaA, Weinheim

[21] J. McBreen, *J. Electroanal. Chem. Interfacial Electrochem.* **1984**, *168*, 415.
[22] J. Winsberg, T. Janoschka, S. Morgenstern, T. Hagemann, S. Muench, G. Hauffman, J. F. Gohy, M. D. Hager, U. S. Schubert, *Adv. Mater.* **2016**, *28*, 2238.
[23] J. Winsberg, T. Hagemann, T. Janoschka, M. D. Hager, U. S. Schubert, *Angew. Chem., Int. Ed.* **2017**, *56*, 686.
[24] T. Janoschka, N. Martin, U. Martin, C. Friebe, S. Morgenstern, H. Hiller, M. D. Hager, U. S. Schubert, *Nature* **2015**, *527*, 78.
[25] M. R. Gerhardt, L. Tong, R. Gómez-Bombarelli, Q. Chen, M. P. Marshak, C. J. Galvin, A. Aspuru-Guzik, R. G. Gordon, M. J. Aziz, *Adv. Energy Mater.* **2017**, *7*, 1601488.
[26] Z. Yang, L. Tong, D. P. Tabor, E. S. Beh, M.-A. Goulet, D. De Porcellinis, A. Aspuru-Guzik, R. G. Gordon, M. J. Aziz, *Adv. Energy Mater.* **2018**, *8*, 1702056.
[27] A. Orita, M. G. Verde, M. Sakai, Y. S. Meng, *Nat. Commun.* **2016**, *7*, 13230.
[28] K. Lin, Q. Chen, M. R. Gerhardt, L. Tong, S. B. Kim, L. Eisenach, A. W. Valle, D. Hardee, R. G. Gordon, M. J. Aziz, M. P. Marshak, *Science* **2015**, *349*, 1529.
[29] Z. Yuan, X. Zhu, M. Li, W. Lu, X. Li, H. Zhang, *Angew. Chem., Int. Ed.* **2016**, *55*, 3058.
[30] Z. Yuan, Y. Duan, H. Zhang, X. Li, H. Zhang, I. Vankelecom, *Energy Environ. Sci.* **2016**, *9*, 441.
[31] B. Huskinson, M. P. Marshak, C. Suh, S. Er, M. R. Gerhardt, C. J. Galvin, X. Chen, A. Aspuru-Guzik, R. G. Gordon, M. J. Aziz, *Nature* **2014**, *505*, 195.
[32] K. Gong, F. Xu, J. B. Grunewald, X. Ma, Y. Zhao, S. Gu, Y. Yan, *ACS Energy Lett.* **2016**, *1*, 89.
[33] S. Eckroad, *Vanadium Redox Flow Batteries: An In-Depth Analysis*, Report 1014836, Electric Power Research Institute, Palo Alto, CA **2007**.
[34] D. W. McComsey, *Handbook of Batteries*, 3rd ed., Vol. *8*, McGraw Hill, New York **2002**, pp. 184–228.
[35] Y. Li, H. Dai, *Chem. Soc. Rev.* **2014**, *43*, 5257.
[36] M. Xu, D. G. Ivey, Z. Xie, W. Qu, *J. Power Sources* **2015**, *283*, 358.
[37] V. Caramia, B. Bozzini, *Mater. Renewable Sustainable Energy* **2014**, *3*, 28.
[38] H. S. Lim, A. M. Lackner, R. C. Knechtli, *J. Electrochem. Soc.* **1977**, *124*, 1154.
[39] Z. Yang, J. Zhang, M. C. Kintner-Meyer, X. Lu, D. Choi, J. P. Lemmon, J. Liu, *Chem. Rev.* **2011**, *111*, 3577.
[40] J.-D. Jeon, H. S. Yang, J. Shim, H. S. Kim, J. H. Yang, *Electrochim. Acta* **2014**, *127*, 397.
[41] C. J. Rydh, B. A. Sandén, *Energy Convers. Manage.* **2005**, *46*, 1957.
[42] J. H. Yang, H. S. Yang, H. W. Ra, J. Shim, J.-D. Jeon, *J. Power Sources* **2015**, *275*, 294.
[43] M. C. Wu, T. S. Zhao, H. R. Jiang, Y. K. Zeng, Y. X. Ren, *J. Power Sources* **2017**, *355*, 62.
[44] K. Lin, R. Gómez-Bombarelli, E. S. Beh, L. Tong, Q. Chen, A. Valle, A. Aspuru-Guzik, M. J. Aziz, R. G. Gordon, *Nat. Energy* **2016**, *1*, 16102.
[45] T. A. Edison, *US Patent 678722*, **1901**.
[46] D. R. Martin, *J. Chem. Educ.* **1948**, *25*, 495.
[47] J. Cheng, L. Zhang, Y.-S. Yang, Y.-H. Wen, G.-P. Cao, X.-D. Wang, *Electrochem. Commun.* **2007**, *9*, 2639.
[48] Y. Cheng, Q. Lai, X. Li, X. Xi, Q. Zheng, C. Ding, H. Zhang, *Electrochim. Acta* **2014**, *145*, 109.
[49] D. E. Turney, M. Shmukler, K. Galloway, M. Klein, Y. Ito, T. Sholklapper, J. W. Gallaway, M. Nyce, S. Banerjee, *J. Power Sources* **2014**, *264*, 49.
[50] Y. Cheng, H. Zhang, Q. Lai, X. Li, D. Shi, *Electrochim. Acta* **2013**, *105*, 618.
[51] Y. F. Yuan, X. H. Xia, J. B. Wu, J. L. Yang, Y. B. Chen, S. Y. Guo, *Electrochim. Acta* **2011**, *56*, 2627.
[52] S. Klaus, Y. Cai, M. W. Louie, L. Trotochaud, A. T. Bell, *J. Phys. Chem. C* **2015**, *119*, 7243.
[53] C.-C. Hu, K.-H. Chang, T.-Y. Hsu, *J. Electrochem. Soc.* **2008**, *155*, F196.
[54] L. F. Arenas, A. Loh, D. P. Trudgeon, X. Li, C. Ponce de León, F. C. Walsh, *Renewable Sustainable Energy Rev.* **2018**, *90*, 992.
[55] Q. Lai, H. Zhang, X. Li, L. Zhang, Y. Cheng, *J. Power Sources* **2013**, *235*, 1.
[56] K. Gong, X. Ma, K. M. Conforti, K. J. Kuttler, J. B. Grunewald, K. L. Yeager, M. Z. Bazant, S. Gu, Y. Yan, *Energy Environ. Sci.* **2015**, *8*, 2941.
[57] G.-M. Weng, Z. Li, G. Cong, Y. Zhou, Y.-C. Lu, *Energy Environ. Sci.* **2017**, *10*, 735.
[58] C. Xie, Y. Liu, W. Lu, H. Zhang, X. Li, *Energy Environ. Sci.* **2019**, *12*, 1834.
[59] Z. Yuan, Y. Duan, T. Liu, H. Zhang, X. Li, *iScience* **2018**, *3*, 40.
[60] Z. Xie, Q. Su, A. Shi, B. Yang, B. Liu, J. Chen, X. Zhou, D. Cai, L. Yang, *J. Energy Chem.* **2016**, *25*, 495.
[61] C. Xie, Y. Duan, W. Xu, H. Zhang, X. Li, *Angew. Chem., Int. Ed.* **2017**, *56*, 14953.
[62] J. Winsberg, C. Stolze, A. Schwenke, S. Muench, M. D. Hager, U. S. Schubert, *ACS Energy Lett.* **2017**, *2*, 411.
[63] C. Wang, Q. Lai, P. Xu, D. Zheng, X. Li, H. Zhang, *Adv. Mater.* **2017**, *29*, 1605815.
[64] C. Xie, H. Zhang, W. Xu, W. Wang, X. Li, *Angew. Chem.* **2018**, *130*, 11341.
[65] Z. Yuan, X. Liu, W. Xu, Y. Duan, H. Zhang, X. Li, *Nat. Commun.* **2018**, *9*, 3731.
[66] S. Selverston, R. F. Savinell, J. S. Wainright, *J. Electrochem. Soc.* **2017**, *164*, A1069.
[67] C. Ding, H. Zhang, X. Li, T. Liu, F. Xing, *J. Phys. Chem. Lett.* **2013**, *4*, 1281.
[68] W. Wang, S. Kim, B. Chen, Z. Nie, J. Zhang, G.-G. Xia, L. Li, Z. Yang, *Energy Environ. Sci.* **2011**, *4*, 4068.
[69] P. K. Leung, C. Ponce-de-León, C. T. J. Low, A. A. Shah, F. C. Walsh, *J. Power Sources* **2011**, *196*, 5174.
[70] P. Pei, K. Wang, Z. Ma, *Appl. Energy* **2014**, *128*, 315.
[71] Y. G. Li, H. J. Dai, *Chem. Soc. Rev.* **2014**, *43*, 5257.
[72] A. R. Mainar, O. Leonet, M. Bengoechea, I. Boyano, I. de Meatza, A. Kvasha, A. Guerfi, J. Alberto Blázquez, *Int. J. Energy Res.* **2016**, *40*, 1032.
[73] Y. Ein-Eli, M. Auinat, D. Starosvetsky, *J. Power Sources* **2003**, *114*, 330.
[74] J. Pan, Y. Y. Xu, H. Yang, Z. Dong, H. Liu, B. Y. Xia, *Adv. Sci.* **2018**, *5*, 1700691.
[75] J. Fu, Z. P. Cano, M. G. Park, A. Yu, M. Fowler, Z. Chen, *Adv. Mater.* **2017**, *29*, 1604685.
[76] Z. Liu, T. Cui, G. Pulletikurthi, A. Lahiri, T. Carstens, M. Olschewski, F. Endres, *Angew. Chem., Int. Ed.* **2016**, *55*, 2889.
[77] J. F. Parker, C. N. Chervin, E. S. Nelson, D. R. Rolison, J. W. Long, *Energy Environ. Sci.* **2014**, *7*, 1117.
[78] S. J. Banik, R. Akolkar, *J. Electrochem. Soc.* **2013**, *160*, D519.
[79] J. F. Parker, C. N. Chervin, I. R. Pala, M. Machler, M. F. Burz, J. W. Long, D. R. Rolison, *Science* **2017**, *356*, 415.
[80] K. W. Knehr, S. Biswas, D. A. Steingart, *J. Electrochem. Soc.* **2017**, *164*, A3101.
[81] A. Mitha, A. Z. Yazdi, M. Ahmed, P. Chen, *ChemElectroChem* **2018**, *5*, 2409.
[82] W. Q. a. T. T. N. Shaigan, *ECS Trans.* **2010**, *28*, 35.
[83] P. Xu, C. Xie, C. Wang, Q. Lai, W. Wang, H. Zhang, X. Li, *Chem. Commun.* **2018**, *54*, 11626.
[84] S. Biswas, A. Senju, R. Mohr, T. Hodson, N. Karthikeyan, K. W. Knehr, A. G. Hsieh, X. Yang, B. E. Koel, D. A. Steingart, *Energy Environ. Sci.* **2017**, *10*, 114.
[85] K. W. Knehr, R. Buline, T. Baldwin, E. Guzman, H. Huynh, R. E. Ciez, D. A. Steingart, *J. Electrochem. Soc.* **2018**, *165*, A4041.
[86] T. H. Wu, Y. Zhang, Z. D. Althouse, N. Liu, *Mater. Today Nano* **2019**, *6*, 100032.

© 2019 WILEY-VCH Verlag GmbH & Co. KGaA, Weinheim

[87] Z. Li, G. Weng, Q. Zou, G. Cong, Y.-C. Lu, *Nano Energy* **2016**, *30*, 283.
[88] Y. K. Zeng, T. S. Zhao, X. L. Zhou, L. Wei, H. R. Jiang, *J. Power Sources* **2016**, *330*, 55.
[89] E. S. Beh, D. De Porcellinis, R. L. Gracia, K. T. Xia, R. G. Gordon, M. J. Aziz, *ACS Energy Lett.* **2017**, *2*, 639.
[90] B. Hu, C. Debruler, Z. Rhodes, T. Liu, *J. Am. Chem. Soc.* **2017**, *139*, 1207.
[91] T. Janoschka, N. Martin, M. D. Hager, U. S. Schubert, *Angew. Chem., Int. Ed.* **2016**, *55*, 14427.
[92] T. Liu, X. Wei, Z. Nie, V. Sprenkle, W. Wang, *Adv. Energy Mater.* **2016**, *6*, 1501449.
[93] J. Luo, B. Hu, C. Debruler, T. L. Liu, *Angew. Chem., Int. Ed.* **2018**, *57*, 231.
[94] X. Li, H. Zhang, Z. Mai, H. Zhang, I. Vankelecom, *Energy Environ. Sci.* **2011**, *4*, 1147.
[95] X. L. Zhou, Y. K. Zeng, X. B. Zhu, L. Wei, T. S. Zhao, *J. Power Sources* **2016**, *325*, 329.
[96] X. L. Zhou, T. S. Zhao, Y. K. Zeng, L. An, L. Wei, *J. Power Sources* **2016**, *329*, 247.
[97] C. Wang, X. Li, X. Xi, W. Zhou, Q. Lai, H. Zhang, *Nano Energy* **2016**, *21*, 217.
[98] G. B. Adams (Google), *U.S. Patent 4,180,623[P]*, **1979**.
[99] F. Xiong, D. Zhou, Z. Xie, Y. Chen, *Appl. Energy* **2012**, *99*, 291.
[100] Z. Xie, Q. Liu, Z. Chang, X. Zhang, *Electrochim. Acta* **2013**, *90*, 695.
[101] Y. Cheng, X. Xi, D. Li, X. Li, Q. Lai, H. Zhang, *RSC Adv.* **2015**, *5*, 1772.
[102] L. J. Junqing Pan, Y. Sun, P. Wan, J. Cheng, Y. Yang, M. Fan, *Electrochem. Commun.* **2009**, *11*, 2191.
[103] Y. Cheng, D. Li, L. Shi, Z. Xiang, *Nano Energy* **2018**, *47*, 361.
[104] B. Li, Z. Nie, M. Vijayakumar, G. Li, J. Liu, V. Sprenkle, W. Wang, *Nat. Commun.* **2015**, *6*, 6303.
[105] J. Zhang, G. Jiang, P. Xu, A. Ghorbani Kashkooli, M. Mousavi, A. Yu, Z. Chen, *Energy Environ. Sci.* **2018**, *11*, 2010.
[106] H. R. Jiang, M. C. Wu, Y. X. Ren, W. Shyy, T. S. Zhao, *Appl. Energy* **2018**, *213*, 366.
[107] Y. Munaiah, S. Dheenadayalan, P. Ragupathy, V. K. Pillai, *ECS J. Solid State Sci. Technol.* **2013**, *2*, M3182.
[108] P. K. Leung, C. Ponce-de-León, C. T. J. Low, F. C. Walsh, *Electrochim. Acta* **2011**, *56*, 6536.
[109] Y. Munaiah, S. Suresh, S. Dheenadayalan, V. K. Pillai, P. Ragupathy, *J. Phys. Chem. C* **2014**, *118*, 14795.
[110] L. Zhang, J. Cheng, Y.-s. Yang, Y.-h. Wen, X.-d. Wang, G.-p. Cao, *J. Power Sources* **2008**, *179*, 381.
[111] B. Li, J. Liu, Z. Nie, W. Wang, D. Reed, J. Liu, P. McGrail, V. Sprenkle, *Nano Lett.* **2016**, *16*, 4335.
[112] P. Arora, Z. Zhang, *Chem. Rev.* **2004**, *104*, 4419.
[113] M. Park, J. Ryu, W. Wang, J. Cho, *Nat. Rev. Mater.* **2017**, *2*, 16080.
[114] J. Winsberg, S. Muench, T. Hagemann, S. Morgenstern, T. Janoschka, M. Billing, F. H. Schacher, G. Hauffman, J.-F. Gohy, S. Hoeppener, M. D. Hager, U. S. Schubert, *Polym. Chem.* **2016**, *7*, 1711.
[115] R. Kim, H. G. Kim, G. Doo, C. Choi, S. Kim, J. H. Lee, J. Heo, H. Y. Jung, H. T. Kim, *Sci. Rep.* **2017**, *7*, 10503.
[116] E. Lancry, B. Z. Magnes, I. Ben-David, M. Freiberg, *ECS Trans.* **2013**, *53*, 107.
[117] S. Chang, J. Ye, W. Zhou, C. Wu, M. Ding, Y. Long, Y. Cheng, C. Jia, *Surf. Coat. Technol.* **2019**, *358*, 190.
[118] O. I. Deavin, S. Murphy, A. L. Ong, S. D. Poynton, R. Zeng, H. Herman, J. R. Varcoe, *Energy Environ. Sci.* **2012**, *5*, 8584.
[119] C. G. Arges, V. Ramani, *Proc. Natl. Acad. Sci. USA* **2013**, *110*, 2490.
[120] G. Couture, A. Alaaeddine, F. Boschet, B. Ameduri, *Prog. Polym. Sci.* **2011**, *36*, 1521.
[121] J. Hu, H. Zhang, W. Xu, Z. Yuan, X. Li, *J. Membr. Sci.* **2018**, *566*, 8.
[122] T. Jiang, *Int. J. Electrochem. Sci.* **2018**, *13*, 5603.
[123] T. Liu, X. Li, H. Zhang, J. Chen, *J. Energy Chem.* **2018**, *27*, 1292.
[124] T. Liu, X. Li, C. Xu, H. Zhang, *ACS Appl. Mater. Interfaces* **2017**, *9*, 4626.
[125] D. U. Lee, J. Y. Choi, K. Feng, H. W. Park, Z. Chen, *Adv. Energy Mater.* **2014**, *4*, 1301389.
[126] S. Li, C. Cheng, X. Zhao, J. Schmidt, A. Thomas, *Angew. Chem., Int. Ed.* **2018**, *57*, 1856.
[127] W. Li, J. Liu, C. Yan, *Carbon* **2011**, *49*, 3463.
[128] L. Yue, W. Li, F. Sun, L. Zhao, L. Xing, *Carbon* **2010**, *48*, 3079.
[129] W. Wang, X. Wang, *Electrochim. Acta* **2007**, *52*, 6755.
[130] T. Liu, X. Li, H. Nie, C. Xu, H. Zhang, *J. Power Sources* **2015**, *286*, 73.
[131] B. Li, M. Gu, Z. Nie, Y. Shao, Q. Luo, X. Wei, X. Li, J. Xiao, C. Wang, V. Sprenkle, *Nano Lett.* **2013**, *13*, 1330.
[132] J.-S. Lee, S. Tai Kim, R. Cao, N.-S. Choi, M. Liu, K. T. Lee, J. Cho, *Adv. Energy Mater.* **2011**, *1*, 34.
[133] P. Gu, M. Zheng, Q. Zhao, X. Xiao, H. Xue, H. Pang, *J. Mater. Chem. A* **2017**, *5*, 7651.
[134] A. Vu, Y. Qian, A. Stein, *Adv. Energy Mater.* **2012**, *2*, 1056.
[135] L. L. Zhang, X. Zhao, *Chem. Soc. Rev.* **2009**, *38*, 2520.
[136] M. Zhou, M. Chi, J. Luo, H. He, T. Jin, *J. Power Sources* **2011**, *196*, 4427.
[137] J. Xiao, D. Mei, X. Li, W. Xu, D. Wang, G. L. Graff, W. D. Bennett, Z. Nie, L. V. Saraf, I. A. Aksay, *Nano Lett.* **2011**, *11*, 5071.
[138] P. G. Bruce, S. A. Freunberger, L. J. Hardwick, J.-M. Tarascon, *Nat. Mater.* **2012**, *11*, 19.
[139] C. Wang, Q. Lai, K. Feng, P. Xu, X. Li, H. Zhang, *Nano Energy* **2018**, *44*, 240.
[140] L. Zhang, H. Zhang, Q. Lai, X. Li, Y. Cheng, *J. Power Sources* **2013**, *227*, 41.
[141] P. Leung, C. P. De León, F. Walsh, *Electrochem. Commun.* **2011**, *13*, 770.
[142] P. Leung, C. P. de León, C. Low, F. Walsh, *Electrochim. Acta* **2011**, *56*, 2145.
[143] P. Leung, C. P. de Leon, F. Walsh, *Electrochim. Acta* **2012**, *80*, 7.
[144] P. Leung, C. Ponce-de-León, F. Recio, P. Herrasti, F. Walsh, *J. Appl. Electrochem.* **2014**, *44*, 1025.
[145] G. Nikiforidis, L. Berlouis, D. Hall, D. Hodgson, *J. Power Sources* **2013**, *243*, 691.
[146] Z. P. Xie, F. J. Xiong, D. B. Zhou, *Adv. Mater. Res.* **2011**, *279*, 451.
[147] G. Sacchetto, P. Pastore, G. Favaro, M. Fiorani, *Anal. Chim. Acta* **1992**, *258*, 99.
[148] P. Kiekens, L. Steen, H. Donche, E. Temmerman, *Electrochim. Acta* **1981**, *26*, 841.
[149] P. Modiba, A. Crouch, *J. Appl. Electrochem.* **2008**, *38*, 1293.
[150] Y. Liu, X. Xia, H. Liu, *J. Power Sources* **2004**, *130*, 299.
[151] R. Bonewitz, G. Schmid, *J. Electrochem. Soc.* **1970**, *117*, 1367.
[152] Z. Xie, B. Yang, D. Cai, L. Yang, *J. Rare Earths* **2014**, *32*, 973.
[153] G. Nikiforidis, L. Berlouis, D. Hall, D. Hodgson, *Electrochim. Acta* **2013**, *113*, 412.
[154] G. Nikiforidis, L. Berlouis, D. Hall, D. Hodgson, *Electrochim. Acta* **2014**, *125*, 176.
[155] W. Lei, Y.-P. Deng, G. Li, Z. P. Cano, X. Wang, D. Luo, Y. Liu, D. Wang, Z. Chen, *ACS Catal.* **2018**, *8*, 2464.
[156] Z. Ma, K. Wang, Y. Qiu, X. Liu, C. Cao, Y. Feng, P. Hu, *Energy* **2018**, *143*, 43.
[157] C. Liu, Y. Li, *J. Alloys Compd.* **2009**, *478*, 415.
[158] Y. Ito, M. Nyce, R. Plivelich, M. Klein, S. Banerjee, *J. Power Sources* **2011**, *196*, 6583.
[159] G. A. Snook, N. W. Duffy, A. G. Pandolfo, *J. Power Sources* **2007**, *168*, 513.
[160] H. B. Li, M. H. Yu, F. X. Wang, P. Liu, Y. Liang, J. Xiao, C. X. Wang, Y. X. Tong, G. W. Yang, *Nat. Commun.* **2013**, *4*, 1894.
[161] Y. Cheng, H. Zhang, Q. Lai, X. Li, D. Shi, L. Zhang, *J. Power Sources* **2013**, *241*, 196.

© 2019 WILEY-VCH Verlag GmbH & Co. KGaA, Weinheim

[162] A. F. Sammells, *U.S. Patent 4,341,847[P]*, **1982**.
[163] T. Wang, M. Yang, J. Pan, *Int. J. Electrochem. Sci.* **2017**, *12*, 6022.
[164] H. Chen, G. Cong, Y. C. Lu, *J. Energy Chem.* **2018**, *27*, 1304.
[165] K. Gong, Q. Fang, S. Gu, S. F. Y. Li, Y. Yan, *Energy Environ. Sci.* **2015**, *8*, 3515.
[166] X. Xi, X. Li, C. Wang, Q. Lai, Y. Cheng, W. Zhou, C. Ding, H. Zhang, *ChemPlusChem* **2015**, *80*, 382.
[167] M. C. Wu, T. S. Zhao, L. Wei, H. R. Jiang, R. H. Zhang, *J. Power Sources* **2018**, *384*, 232.
[168] P. T. Daniel, G.-B. Rafael, T. Liuchuan, G. G. Roy, J. A. Michael, A.-G. Alan, ChemRxiv, preprint **2018**, https://doi.org/10.26434/chemrxiv.6990053.v2.
[169] C. Ding, X. Ni, X. Li, X. Xi, X. Han, X. Bao, H. Zhang, *Electrochim. Acta* **2015**, *164*, 307.
[170] D. P. Tabor, R. Gómez-Bombarelli, L. Tong, R. G. Gordon, M. J. Aziz, A. Aspuru-Guzik, *J. Mater. Chem. A* **2019**, *7*, 12833.
[171] M. H. Chakrabarti, R. A. W. Dryfe, E. P. L. Roberts, *Electrochim. Acta* **2007**, *52*, 2189.
[172] X. Wei, L. Cosimbescu, W. Xu, J. Z. Hu, M. Vijayakumar, J. Feng, M. Y. Hu, X. Deng, J. Xiao, J. Liu, V. Sprenkle, W. Wang, *Adv. Energy Mater.* **2015**, *5*, 1400678.
[173] M. L. Perry, A. Z. Weber, *J. Electrochem. Soc.* **2016**, *163*, A5064.
[174] D. Bryans, B. G. McMillan, M. Spicer, A. Wark, L. Berlouis, *J. Electrochem. Soc.* **2017**, *164*, A3342.
[175] M. Schneider, G. P. Rajarathnam, M. E. Easton, A. F. Masters, T. Maschmeyer, A. M. Vassallo, *RSC Adv.* **2016**, *6*, 110548.
[176] D. Desai, X. Wei, D. A. Steingart, S. Banerjee, *J. Power Sources* **2014**, *256*, 145.
[177] J.-J. Han, N. Li, T.-Y. Zhang, *J. Power Sources* **2009**, *193*, 885.
[178] J. Cheng, Y. Wen, Y. Xu, G. Cao, Y. Yang, *Chem. J. Chin. Univ.-Chin.* **2011**, *32*, 2640.
[179] M. F. de Carvalho, I. A. Carlos, *Electrochim. Acta* **2013**, *113*, 229.
[180] Y. Ito, M. Nyce, R. Plivelich, M. Klein, D. Steingart, S. Banerjee, *J. Power Sources* **2011**, *196*, 2340.
[181] Y. Ito, X. Wei, D. Desai, D. Steingart, S. Banerjee, *J. Power Sources* **2012**, *211*, 119.
[182] Y. Wen, T. Wang, J. Cheng, J. Pan, G. Cao, Y. Yang, *Electrochim. Acta* **2012**, *59*, 64.
[183] Y.-h. Wen, J. Cheng, L. Zhang, X. Yan, Y.-s. Yang, *J. Power Sources* **2009**, *193*, 890.
[184] M. Park, E. S. Beh, E. M. Fell, Y. Jing, E. F. Kerr, D. De Porcellinis, M. A. Goulet, J. Ryu, A. A. Wong, R. G. Gordon, *Adv. Energy Mater.* **2019**, 1900694.
[185] S. Gu, K. Gong, E. Z. Yan, Y. Yan, *Energy Environ. Sci.* **2014**, *7*, 2986.

© 2019 WILEY-VCH Verlag GmbH & Co. KGaA, Weinheim